A Method for Interpreting the *In-Situ* Consolidation State of Surficial Seabed Sediments using a Free-Fall Penetrometer

Jared Dorvinen

Thesis submitted to the Faculty of the
Virginia Polytechnic Institute and State University
in partial fulfillment of the requirements for the degree of

Master of Science
in
Civil Engineering

Nina Stark, Chair
Bernardo Castellanos
Jennifer L. Irish

September 1, 2016
Blacksburg, Virginia

Keywords: Free-Fall Penetrometer, Marine Clay, Self-weight Consolidation, Erosion

A Method for Interpreting the *In-Situ* Consolidation State of Surficial Seabed Sediments using a Free-Fall Penetrometer

Jared Dorvinen

ABSTRACT (academic)

Free-fall penetrometers (FFP) are useful instruments for the rapid characterization of seabed sediments. However, the interpretation of FFP data remains largely a skilled task. In order to increase the reliability of results obtained using these instruments, in both expert and non-expert hands, it is advantageous to establish well defined and repeatable procedures for instrument use and data interpretation. The purpose of this research was therefore to develop and refine methods for the interpretation of FFP data.

Data were gathered with the FFP *Nimrod* during two surveys following dredging in Sydney Harbour, Nova Scotia. The challenge of interpreting the data from these two surveys in an efficient and consistent manner was the basis of this work and led to the development of new techniques for improving resolution of the mud-line, identifying areas of erosion and deposition, and qualitatively evaluating the consolidation state of cohesive marine sediments.

The method developed for improving the resolution of the mud-line simply describes a procedure of combining the data from different accelerometers with different accuracies and ranges to more clearly define the point of impact with the seafloor. The method developed to evaluate *in-situ* sediment consolidation state combines theories of self-weight consolidation and ultimate bearing capacity to predict a range of potential bearing capacities for normally consolidated cohesive sediments. Finally, by combining the previous two methods a third method is proposed for locating areas of potential erosion and deposition.

A Method for Interpreting the *In-Situ* Consolidation State of Surficial Seabed Sediments using a Free-Fall Penetrometer

Jared Dorvinen

ABSTRACT (public)

Human interaction with the marine environment takes many forms. For example, in the case of marine/civil engineering projects these interaction may include: erecting off-shore wind turbines, installing oil rigs, and building break waters. All of these activities involve installing structures with foundations on or attached to the seafloor. In order for these structures to be effective and for there foundation to not fail a knowledge of the physical conditions *at* the seafloor is required.

Physical characterization of the seafloor involves describing three interdependent processes: hydrodynamics (the movement of water), morphodynamics (the dynamic processes which shape the seafloor), and sediment dynamics (the movement of sediments). Together, these three form a complex and interacting feedback loop in which a change in one will affect the states of the others and eventually itself. For example, energetic hydrodynamic conditions may erode sediment from the seabed. As this sediment is transported and deposited elsewhere by the flow of water, the initial features which make up the seafloor, such as dunes, ripples, and sand-waves, are reshaped. These forms may grow or shrink, migrate, or be wiped out and replaced entirely. The changed shape of the seabed will then in turn influence the flow of passing waves, tides, and currents. The newly changed flow patterns then restarting the cycle anew. Understanding the interactions of these processes is vital to designing effective engineering works in the marine environment.

Free-fall penetrometers (FFP) are useful instruments for the rapid characterization of seabed sediments and can therefore provide information about the sediment dynamics at the seafloor's surface. However, the interpretation of FFP data remains largely a skilled task. In order to increase the reliability of results obtained using these instruments, in both expert and non-expert hands, it is advantageous to establish well defined and repeatable procedures for instrument use and data interpretation. The purpose of this research was therefore to develop and refine methods for the interpretation of FFP data.

During two surveys in Sydney Harbour, Nova Scotia, data were gathered from the seafloor's surface with the FFP *Nimrod*. The challenge of interpreting this data in an efficient and consistent manner was the basis of this work and resulted in the development of new methods and techniques for data interpretation and analysis. These methods will allow for the improved characterization of sediment processes and properties at the uppermost seafloor, contributing to a better understanding of the seafloor environment as a whole and improving engineering designs.

Acknowledgments

I would like to extend my gratitude to my advisor, Dr. Nina Stark, for her support and guidance with this project. I would also like to thank her for her encouragement to publish and present research at conferences and to help me recognize and achieve my fullest potential. I would also like to thank Dr. Bernardo Castellanos and Dr. Jennifer Irish for serving on my committee, as well as Dr. Thomas Brandon for providing advice and guidance.

The Virginia Tech Charles E. Via Department of Civil and Environmental Engineering, the Sydney Ports Corporation, and Cape Breton University are recognized for funding this research. I thank Alex E. Hay (Dalhousie University) and Dave Woodland (Cape Breton University) for support with the study as well as Christian Zoellner (MARUM) for technical support and assistance with the *Nimrod* logistics.

Furthermore, my appreciation is extended to the coauthors of the two manuscripts: Nina Stark (Virginia Tech), Bruce Hatcher (Cape Breton University), Matthew Hatcher (Dalhousie University), Vincent Leys (CBCL Limited), and Achim Kopf (MARUM).

I am thankful for the support and encouragement of my family throughout my academic training and extend my deepest gratitude to my best friend, Rebecca.

Contents

List of Figures

List of Tables

Nomenclature

Abbreviations

ASTM	American Society for Testing and Materials
CDF	Confined sediment disposal facility
DP1	penetration depth at *qsbc* of 1 kPa (equivalent to TLT)
FFP	Free-Fall Penetrometer
GPS	Global Positioning System
kPa	kilo-Pascal = 1000 Pascals ($\frac{N}{m^2}$)
kHz	kilo-Hertz = 1000 cycles per second (Hertz)
LIR	Load Increment Ratio
LL	Liquid Limit
MEMS	MircoElectroMechanical Systems
PAH	polycyclic aromatic hydrocarbons
PCB	polychlorinated biphenyls
qsbc	quasi-static bearing capacity (kPa)
SS	Surface Strength, *qsbc* at 10 cm of penetration (equivalent to TS)
TLT	Top Layer Thickness, peneration depth at *qsbc* of 1 kPa (equivalent to DP1)
TS	Top Layer Strength, *qsbc* at 10 cm of penetration (equivalent to SS)
USCS	United Soil Classification System
USR	Undrained Strength Ratio
WAAS	Wide Area Augmentation System

Symbols

A	bearing area of FFP
B	characteristic diameter of the FFP
c	cohesion (kPa)
C_C	compression index
dec	deceleration in units of gravity
d_{50}	mass-median diameter grain-size
e_{1kPa}	void ratio at 1 kPa of vertical effective stress
F_{sr}	sediment resistance force
g	Earth's gravitational acceleration $\approx 9.81 \frac{m}{sec^2}$
H_{sig}	significant wave height
I_w	plasticity index
K	a newly defined constant
N_c, N_q, N_γ	bearing capacity factors
q_c, q_q, q_γ	bearing capacity due to: cohesion, unit weight of soil, and surcharge
q_u	bearing capacity at failure (kPa)
s_u	undrained shear strength (kPa)

Greek Letters

γ	unit weight of soil
${\sigma_{vo}}'$	vertical effective stress (kPa)
τ_f	shear strength at failure (kPa)
ϕ'	effective angle of internal friction

Chapter 1. Introduction

1.1 Motivation

Human interaction with the marine environment takes many forms, with engineering activities being one important example. When installing structures and performing engineering activities near or on the seafloor a knowledge of the conditions *at* the seafloor is required. In the case of marine/civil engineering projects, three interconnected processes play a major role in the physical characterization of the seafloor: hydrodynamics, morphodynamics, and sediment dynamics. Together, these three form a complex and interacting feedback loop in which a change in one will affect the states of the others and eventually itself (Fig. 1.1). For example, energetic hydrodynamic conditions may lead to the entrainment of sediment, eroding it from the seabed. As this sediment is transported and deposited elsewhere, the initial morphological bedforms, such as dunes, ripples, and sand-waves, are reshaped. These forms may grow or shrink, migrate, or be wiped out and replaced entirely. The changed seabed morphology will then in turn influence the hydrodynamics of waves, tides, and currents passing or flowing in their vicinity. The newly changed hydrodynamic conditions then restart the cycle anew, further changing the state of the system (e.g. Ashley 1990; García 2008).

When considering hydrodynamics in marine engineering applications, focus is placed on describing the stresses imposed on structures by hydrodynamic loading, how the presence of those structures affects the hydrodynamics, and how the effected hydrodynamics interact with sediment transport processes. Because of this, describing the flow field by measuring current velocity, turbulence, and water levels is important. These measurement are often made through the use of acoustic Doppler current profilers (ADCPs), acoustic Doppler velocimeters (ADVs), pressure gauges, tide gauges, and wave rider buoys (e.g. Thompson and Emery 2014). The modeling of hydrodynamic conditions using computer algorithms is a highly developed and advancing field. The differential equations that govern these models are all ultimately dependent on the boundary conditions of the system within which they operate (Anderson 1995; Wendt and Anderson 2009). In the marine environment the boundaries happen to include: the bathymetry of the seafloor, the sediment-water interface, and the water surface.

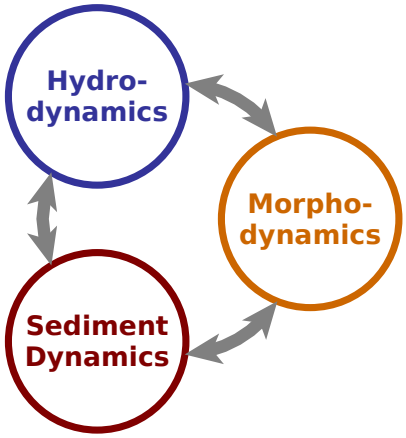

Figure 1.1: The dynamic feedback loop of hydrodynamics, sediment dynamics, and morphodynamics which dominates the seafloor

The study of morphodynamics is concerned with the formation of large-scale sediment features such as dunes, sand waves, ripples, scarps, and sub-aquatic plains, etc. which collectively form the bathymetry of the seafloor. Traditionally, bathymetry was quantified by manual depth soundings, but today it is more commonly measured using acoustic methods such as single as well as multi-beam echo sounders, side-scan sonar, and rotary side-scan sonar (U.S. NOS 2016). More recently LIDAR methods have also been developed which allow for the rapid high resolution mapping of large areas of shallow open water and near-shore coastal bathymetry (e.g. Irish and White 1998).

How the seafloor's bathymetry is formed and changes overtime is the result of both large-scale mass movements (e.g. landslides and tectonic activity) as well as the sediment-scale processes which are the focus of sediment dynamics. Sediment dynamics are governed by erosion and deposition processes, the consolidation and reworking of sediments, along with the composition and strength parameters of the seafloor. Many of these sediment processes and properties are also of great importance to the work of geotechnical engineers. Structures installed in the marine environment require a foundation or moorings, in order to fix their position, usually placed on or attached to the seafloor. Likewise, when dredged material is disposed in the marine environment, and particulates suspended in runoff and river discharge enter the sea, they eventually settle out of suspension and form the fresh top layer of the seafloor. Designing foundations and moorings, managing dredged material, and understanding natural sediment transport processes all require a knowledge of sediment dynamics as well as the material properties of the soil that makes up the seafloor.

There are two principal ways of measuring the properties of seafloor sediments. The first is

by taking samples of the sediment to be later analyzed in the laboratory and the second is to make measurements of these properties *in-situ*. Each of these approaches has their distinct advantages and shortcomings.

There are a variety of methods available for making *in-situ* measurements of the seabed. These include acoustic methods (ADCP, chirp sonar, seismic methods), electric resistivity measurements, optical/x-ray backscatter methods, and penetrometry as well as free-fall penetrometry (Dayal et al. 1975; McAnally et al. 2007b). This thesis is largely concerned with the development of novel methods for interpreting *in-situ* data obtained with free-fall penetrometers.

1.1.1 What is a free-fall penetrometer?

The American Heritage® Science Dictionary (2011) defines a penetrometer as

> *A device for measuring the denseness, compaction, or penetrability of a substance, such as soil, agricultural produce, or semisolid petroleum products. A penetrometer typically measures the resistance of the substance to penetration to a given depth by a weight-driven cone or needle of a given shape.*

These devices have found applications in a variety fields including: measuring fruit ripeness (e.g. Harker et al. 1996), assessing turf quality (e.g. Caple et al. 2012), measuring the toughness of foliage (e.g. Charrett 1968), evaluating the hardness of bitumen for use in asphalt concrete (e.g. ASTM D5/D5M-13), and studying asteroids and comets (e.g. Glaser et al. 2008). However, the principal use of such instruments is in geotechnical engineering and soil mechanics. Cone-tipped penetrometers have been used for cone penetration testing (CPT) since the 1940s on land (Lunne et al. 1997) and since the 1970s for marine applications (Dayal et al. 1973; Lunne 2012). Since the first marine penetrometers used in the 1970s, marine CPT has become an important tool for measuring the properties of seafloor sediments *in-situ* (Lunne 2012).

The main difference between terrestrial and marine penetrometry is the conditions under which measurements are made. Making penetrometer measurements at sea is difficult. Traditionally, land-based CPT is performed by pushing a cone-tipped rod mounted to a large and heavy reaction-frame at a fixed rate of 0.02 m/s into the ground (Lunne et al. 1997). These rigs are mobile and typically mounted to a truck or other vehicle. Methods for performing CPT of this type are well defined and documented in standards (e.g. ASTM-D5778-12). Traditional marine CPT is also performed with reaction-frame based penetrometers. These tests are a close analogue to those performed with terrestrial instruments and therefore benefit from the widespread standardization of these methods and data interpretation (Dayal et al. 1975, Lunne 2010). Additionally, they can be fitted with a variety of sensors and reach penetration depths on the order of 100 meters allowing for high quality characterization of

the seabed for foundation designs (Lunne 2012). However, their large size comes with a few distinct drawbacks. The use of a reaction-frame which is placed on the seafloor disturbs the *in-situ* sediment conditions at the seabed surface and prevents collection of meaningful data from this region. Also, the class of vessel required to deploy such instruments is large and expensive while the process itself is relatively slow.

This led to the idea of portable free-fall penetrometers (FFPs). In contrast to frame-based, engine-driven marine cone penetrometers, FFPs are light weight, easy to deploy, inexpensive, and operable in areas inaccessible to other methods (Denness 1981; Stark et al. 2014b). Due to their smaller size and free-fall deployments, these instruments may be utilized in rougher waters and from smaller vessels. The advantage of these instruments is that their small size allows for very quick surveys of many locations in a small amount of time and under a wide variety of hydrodynamic conditions. However, also due to their relatively small mass and free-fall driven penetration, these cone penetrometers are only suited for examining surficial seabed sediments at penetration depths in the range of meters in soft fine grained sediments and just a few decimeters in sands (Harris et al. 2008; Stark et al. 2009a). An example of a modern portable free-fall penetrometer is shown in Figure 1.2.

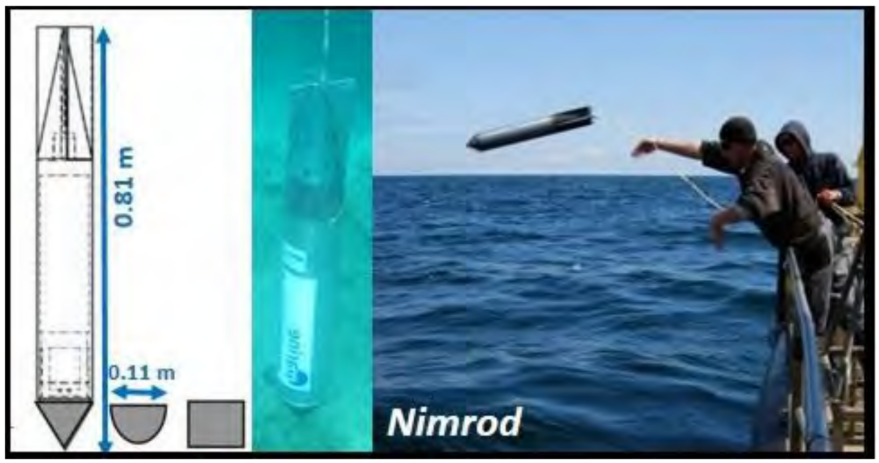

Figure 1.2: The free-fall penetrometer *Nimrod*, modified after Stark et al. (2014b)

1.1.2 Gaps in Knowledge

While the deployment of FFPs may be simple compared to that of their reaction frame-based counterparts, interpretation of the collected data is more complex. Issues such as strain-rate effects (e.g. Chung 2006; Oliveira 2011; Steiner et al. 2013), instrument orientation during impact (e.g. Blake et al. 2016), non-standard tip-geometries (e.g. Mulhearn 2002,2003), and impact detection (e.g. Mulukutla et al. 2011) create difficulties when attempting to obtain meaningful results from FFP data. These complexities require methods specific to FFPs.

A method of interpreting field data must have the following attributes to be considered accurate and defensible: (i) based in theory, (ii) corroborated by laboratory testing, and (iii) verified as repeatable in the field. Aspects of simple field data interpretation with FFPs have been proven by all three methods but there are still certain aspects of data interpretation which remain poorly explained by theories, uncorroborated by laboratory testing, or both. Various authors have identified such uncertainties as a considerable hindrance to the more widespread adoption of FFPs (e.g. Carter and Nazem 2013; Chow and Airey 2013).

In this thesis, data from Sydney Harbour, Nova Scotia was collected during two field surveys with the FFP *Nimrod* (Fig. 1.2) and used as a case study for exploring methods to improve data processing, interpretation, and analysis. Specifically, three methods were developed: one method for improving identification of the point of impact with the seafloor in FFP data and a second to estimate sediment consolidation state directly from FFP data and index properties. The third method was developed by correlating the previous two methods with results from oedometer testing and index properties to identify areas potentially experiencing erosion or deposition in Sydney Harbour. These methods each represents incremental progress in addressing current challenges faced in FFP data interpretation.

1.2 State of the Art

Free-fall penetrometers (FFPs) are useful tools for the rapid characterization of the geotechnical properties of seabed sediments. These instruments are used to estimate the undrained shear strength of surficial seabed sediments, but have also been applied to locate dredged material, identify areas of sediment transport, and estimate sediment consolidation behavior among others (Chow et al. 2014). Some smaller FFPs are quite sensitive to impacts with very soft seafloor sediments, even fluid mud, allowing for high resolution ($\pm$1 cm) measurements of these sediments (e.g. Seifert and Kopf 2012).

Free fall penetrometers may be broken into two main groups: lance-like FFPs (e.g. STING, Poeckert et al. 1997; FFCPT, Osler et al. 2006; LIRmeter, Stephan et al. 2011), and projectile like FFPs (e.g. XBP, Stoll and Akal 1999; *Nimrod*, Stark et al. 2009b; *Blue-Drop*, Stark et al. 2015). Lance-like instruments are typically capable of achieving greater penetration depths than projectile-like instruments. However, projectile-like instruments are hydro-dynamically designed and capable of withstanding more violent impacts with the seafloor than lance-like penetrometers. Examples of various free-fall penetrometers are presented in Table 1.

1.2.1 Measured and Derived Properties

Penetrometers are designed to measure a wide variety of soil parameters during instrument deployment, of which the two most basic parameters are side friction and cone penetration

Table 1.1: Examples of free-fall penetrometers in the literature.

Penetrometer Name	Type and Description	Published Source
STING	Lance-like	Poeckert et al. (1997)
XBP	Projectile-like	Stoll and Akal (1999)
XDP	Projectile-like	Thompson et al. (2002)
FFCPT Lance	Lance-like	Stegmann et al. (2006)
FFCPT	Lance-like	Osler et al. (2006)
Harpoon	Lance-like	Mosher et al. (2007)
Nimrod	Projectile-like	Stark et al. (2009b)
LIRmeter	Lance-like	Stephan et al. (2011)
BlueDrop	Projectile-like	Stark et al. (2015)

resistance. During a test the penetration resistance force of a soil is measured using strain elements located in the penetrometer's sensor tip. This data is used to infer sediment bearing capacity and shear strength (e.g. Lunne et al. 1997; Robertson 2009). Side friction is measured using a friction sleeve connected to load cells and is commonly used to estimate the re-molded shear strength of soils (Lunne 1997; Robertson 2009; Boggess and Robertson 2010).

When using free-fall penetrometers in-place of their frame-based counterparts, often deceleration of the instrument upon impact with the seafloor is measured instead of the cone penetration resistance force. Micro-electro-mechanical systems (MEMS) accelerometers are used to measure deceleration time-series during impact, which is then used to calculate penetration resistance force experienced by the penetrometer during impact. These measurements are recorded using a data logger. Once corrected for the effects of strain-rate and tip-geometry an estimate of shear strength can be made from this data (Dayal 1981; Stoll et al. 2007). In addition to deriving shear strength estimates, the deceleration profile can be used to infer sediment layering (e.g. Stark and Kopf 2011) and classify sediment type (e.g. Stoll et al. 2007). Furthermore, a method for estimating sediment consolidation state from FFP data and exploring how these estimates may be used to identify areas experiencing erosion and deposition is presented in Chapter 3.

The orientation of a free-fall penetrometer is an important parameter to be considered when evaluating an impact with the seafloor. The quality of the penetrometer impact may be verified through the use of 3D MEMS tilt sensors to ensure vertical penetration. These sensors can also be used in conjunction with the impact decelerometers to visualize the entire path of the penetrometer as it falls through the water column and is embedded in the seafloor (e.g. Blake et al. 2016).

CPTu penetrometer sensor systems are commonly used for measurements of pore-pressures in

seabed sediments. These systems use pressure transducers typically positioned either on the face of or behind the penetrometer's cone tip. Placing of the pressure transducer behind the cone tends to produce negative pore pressure readings on impact while placement on the face of the cone will produce high positive pressures (Robertson and Campanella 1983). These measurements are a combination of hydrostatic pressure, preexisting *in-situ* pore-pressures, as well the effects of soil matrix deformation during impact (Stark et al. 2015).

Optical backscatter is also sometimes measured during FFP deployments. To complete these measurements a photo-emitter and photo-receptor are included in the penetrometer. The fraction of the light produced by the photo-emitter which is then detected by the photo-receptor can be used to assess the concentration of suspended material in the water-column as well as help identify the mud line (e.g. Brooke Ocean FFCPT, Osler et al. 2006). Nuclear transmission and backscatter are also used to measure *in-situ* material density in a similar way (e.g. Hirst et al. 1975; Dasari et al. 2006). Electrical resistivity can also be measured by modified CPTs and used as a proxy for water content and porosity (Osler et al. 2006; Dijkstra et al. 2012). Stegmann et al. (2006) among others have also included temperature measurements in the design of penetrometers.

1.2.2 Impact Detection

When focusing on characterizing sediment properties at the seafloor surface, resolving the point of impact accurately is of particular importance. As was noted by Chow and Airey (2014), penetrometers with cone tips have trouble detecting the seabed. This difficulty is problematic as improper detection of the point of impact may lead to calculated bearing capacities which are highly inaccurate until full tip-penetration is achieved. This issue may cause errors in the interpretation of penetrometer data and erroneous results when attempting to quantify processes which occur in this narrow layer of the uppermost seafloor (< 10 cm penetration).

The identification of the point of impact has typically been performed on an impact-by-impact basis by an experienced analyst who manually chooses the point of impact from a time-series of deceleration data based on noticeable deceleration in the data record (Mulukutla et al. 2011). Commonly, data from a single MEMS accelerometer is used to analyze any given penetrometer deployment. The use of a single sensor means that in order to capture the entire impact a sensor with a high capacity must be used. This may lead to fine resolution of the seabed surface being lost.

In order to better understand the importance of impact detection, take for example a penetrometer with a data logger recording at 1 kHz which is moving at 10 m/s. This instrument progresses a distance of 1 cm between each recorded measurement. While this may not seem like much, a one centimeter uncertainty in the assumed penetration depth can have the effect of calculating sediment strengths which are orders of magnitude greater than reality in the first few centimeters of penetration. For example, the effects of improper impact detection

in a FFP deceleration record, either too early or too late, on the derived sediment strength values, represented by quasi-static bearing capacity (*qsbc*), are illustrated in Figure 1.3.

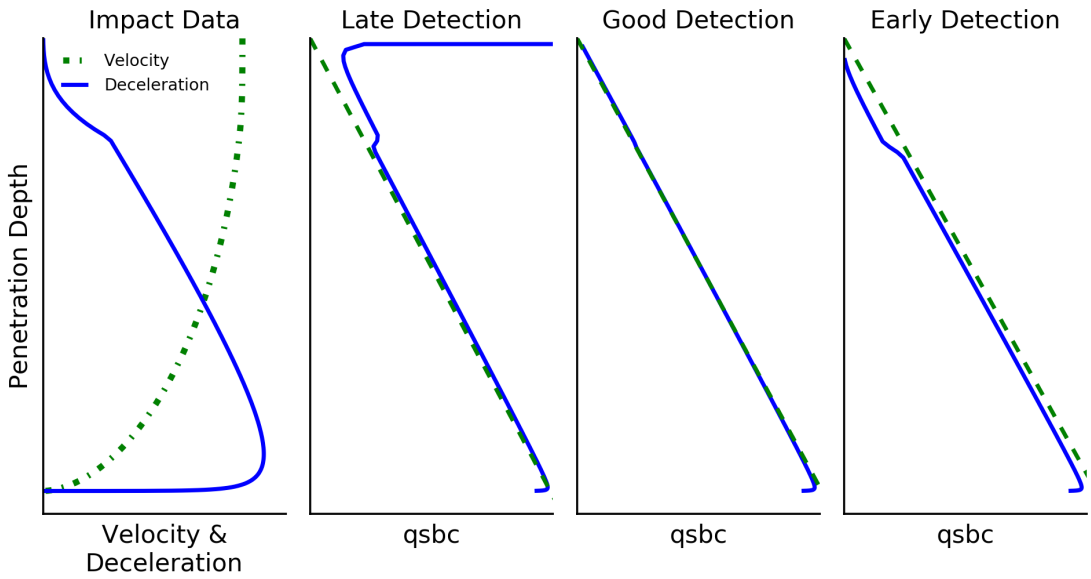

Figure 1.3: Effects of error in FFP impact detection on derived parameters. Shown is the calculated *qsbc* of a hypothetical soil with bearing capacity increasing linearly with depth. Calculated *qsbc* values are represented by the solid lines while the dashed lines signify the known *qsbc*-depth profile. The examples shown are the result of an impact detection occurring a single time step late or four time steps early.

Precise impact detection of a cone tipped FFP with the seafloor is a difficult problem facing the users of these instruments today (Mulukutla et al. 2011; Morton et al. 2015). Currently, data collected prior to full cone insertion is considered useless by various authors (e.g. Chow and Airey 2013; Moavenian et al. 2016). Figure 1.3 shows that based on common data interpretation methods this view may not be unfounded. It is seen that even small errors of a few time steps in impact detection can drastically alter the derived soil strength values, prior to full insertion of the cone in the seabed.

However, it should be noted that three issues may be identified as the cause of most of this error: (i) insufficient accelerometer resolution for detecting the very beginning of seafloor impact, (ii) the distance traveled during the time between measurements taken by the data logger, and (iii) the changing bearing-area of the penetrometer's cone tip during impact. The combination of these three issues leads to a situation of miss-matched bearing areas and deceleration measurements being used to calculate soil strength during the initial stages of seabed impact. When the bearing area is too large, strength is underpredicted, while a bearing area which is too small leads to the over prediction of sediment strengths at the surface.

While issue (iii) could be addressed by using a blunt-nosed penetrometer, the cone-tip is already the standard in conventional CPT testing and deviating from this standard would create problems relating the results of FFP tests to those of conventional CPT. The first two issues on the other hand could be resolved with improvements to accelerometer and data logger technologies. However, in light of the current limitations of these sensors, techniques for improving impact detection with current instrumentation are presented. A technique for addressing insufficient accelerometer resolution is described in Chapter 2 while another for resolving data logger limitations is presented below.

In order to account for data logger produced uncertainty in FFP measurements, consider the following. When a cone impacts the seafloor the first recorded observation of this impact occurs at some time t_i with the FFP moving at a corresponding velocity, v_i, where the subscript i represents the current time-step. However, depending on the impact velocity of the FFP and the data logger's recording rate, it is possible that the cone has actually impacted the seafloor at any time t such that $t_i \geq t > t_{i-1}$. Depending on the impact velocity, the penetrometer will have progressed a corresponding distance, z, anywhere in the range $(t_i - t_{i-1})\frac{v_i+v_{i-1}}{2} \geq z > 0$. The exact point of impact between the two time-steps, t_i and t_{i-1}, is unknown while the probability of the impact occurring at any point between the two is uniform. This means that, on average, the best approximation of the actual time of impact is $\frac{(t_i-t_{i+1})}{2} = \frac{\delta t}{2}$, where δt is the time between recordings taken by the data logger. The depth of penetration at the time impact was detected, z, may then be approximated as $z = \frac{(t_i-t_{i-1})}{2}\frac{(v_i+v_{i-1})}{2} = \delta t\frac{(v_i+v_{i-1})}{4}$ (Haghighat 2014).

In addition to this theoretical basis, there are also practical matters to consider. Given the low resistance force provided by soft materials during the first centimeters of penetration it is likely that the initial point of impact will go undetected. Also, during the course of a long survey a cone may become blunted by impacting with a rock or other hard surface. In both of theses cases the actual average bearing-area corresponding to first point of impact detection will tend to be greater than that predicted by an assumed penetration depth of $z = \delta t\frac{(v_i+v_{i-1})}{4}$. Assuming an error of a single time-step, both conditions would correspond to a penetration depth closer to $z = \delta t(1 + \frac{1}{2})\frac{(v_i+v_{i-1})}{2}$. It is therefore recommended that an initial penetration depth in the range of $\delta t(1 + \frac{1}{2})\frac{(v_i+v_{i-1})}{2} \geq z > \delta t\frac{(v_i+v_{i-1})}{4}$ be used when analyzing cone-tipped FFP impacts. Once full cone insertion is achieved these corrections should have little to no effect on data interpretation. Also, as data loggers and accelerometers continue to improve these issue will become to be less and less important.

1.2.3 State of Consolidation

Identifying sediment consolidation state quickly, accurately, and inexpensively from *in-situ* data is an area of active research and ongoing development. The ability to measure the *in-situ* material density along the vertical profile of the seabed is useful when planning dredging activities, modeling fluid mud and sediment transport behavior, and installing such items

as artificial reefs, torpedo anchors, and submarine pipelines on the seafloor (McAnally et al. 2007a,b; Jia et al. 2013a). Currently various strategies exist to accomplish this goal.

One recently developed method uses a vibrating tuning fork to estimate the density of fluid mud layers (Winterwerp and van Kesteren 2004; Ha et al. 2010). In this method vibrations produced by one leg of the fork are picked up by the other. The frequency of the second leg's response is analyzed based on calibration with samples taken at the site and produces an estimate of density (McAnally et al. 2007b). However, this instrument's design does not allow it to penetrate a consolidated clay or sandy seabed. Acoustic methods may also be used, including a recently developed non-intrusive "micro-chirp" system (Ha et al. 2010) as well as *in-situ* acoustic wave attenuation probes (McAnally et al. 2007b; Ha et al. 2010). While the micro-chirp system does allow for measurements over a larger spatial scale than point measurements common in other techniques, these methods still require calibration of acoustic impedance with sediment samples taken from the field. The accuracy of these methods are also particularly sensitive to the presence of gas bubbles entrained in sediment or the water column (Parker and Kirby 1982; McAnally et al. 2007b; Ha et al. 2011).

Currently, the most accurate methods available for measuring sediment densities *in-situ* are nuclear radiation transmission and backscatter techniques. They operate on the principle that the radiation absorption of sediment is proportional to the density of the material (Hirst et al. 1975). This technique has been incorporated into radioisotope cone penetrometers (RI-CPTs) in two main forms: (i) nuclear-density penetrometers (ND-CPTs) which use a gamma-radiation source, and (ii) neutron-moisture penetrometers (NM-CPTs) which work with neutron-radiation (Dasari et al. 2006). Many examples of these instruments exist in the literature and they have been in use for decades (e.g. Keller 1965; Hirst et al. 1975; Shibata et al. 1992; Dasari et al. 2006; Karthikeyan et al. 2007; Jia et al. 2013a,b). However, drawbacks to these instruments include: a high cost of operation (more than $1000 per test), licensing requirements and restrictions associated with their use, and additional safety measures required to avoid excess radiation exposure during operation (Dasari et al. 2006; McAnally et al. 2007b).

While less precise than nuclear methods, electrical conductivity probes have been successfully used to produce depth density profiles (e.g. Dijkstra et al. 2012). These instruments may have a resolution on the order of centimeters, however they require calibration with material from the deployment site. The operating principle behind these instruments is that pore water is much more conductive than the sediment grains in a soil matrix, therefore a given soil's conductivity is proportional to its water content. While this works well in marine environments, the reliance on the conductivity of pore water to infer sediment porosity makes these instruments not suitable for use in brackish waters where the salinity in surface water and pore-water of sediment layers may not be equivalent (Winterwerp and Van Kesteren 2004; McAnally et al. 2007b). Osler et al (2006) describe an example of an electrical conductivity probe built into a FFP.

One disadvantage all of these methods share is that they require additional sensors to be

included within the existing FFP instrumentation or that an altogether separate instrument be used. These changes to instrumentation have the potential to increase the costs and complexity of surveying. A new method for estimating sediment density *in-situ* using existing FFP data is proposed in Chapter 3.

1.2.4 Erosion and Deposition

Mapping areas of sediment deposition using *in-situ* penetration testing has been accomplished by examining sediment layering evident in FFP deceleration records (e.g. Stark and Kopf 2011; Stark et al. 2014a) as well as simply by examining the overall penetration depth of cones pushed by a known constant force (e.g. Håkanson 1986). However, neither of these approaches explicitly take sediment consolidation state into consideration. Since the seabed surface in areas of sediment erosion tends to be over-consolidated, and conversely the seabed is either normally-consolidated or consolidating in areas of sediment deposition, developing methods to roughly classify the consolidation state of surficial seabed sediments will allow areas of sediment erosion, deposition, and stability to be identified. Figure 1.4 provides a conceptual illustration of the expected effects immediately following erosion and deposition on the strength, $qsbc$, and over consolidation ratio, OCR, of an initially normally consolidated fine grained sediment. The concepts in Figure 1.4 are further explored and used to propose a method for identifying areas of sediment deposition and erosion in Chapter 3.

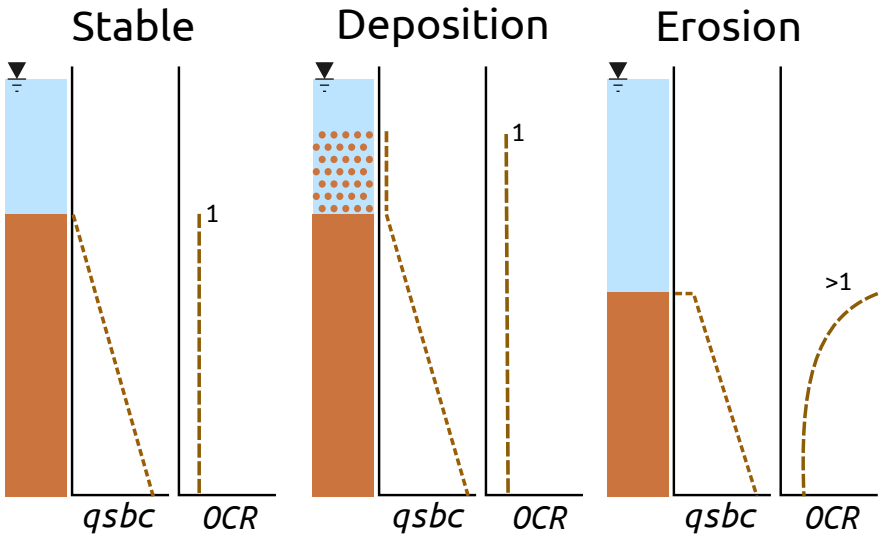

Figure 1.4: Effects of erosion and deposition on the *qsbc* and *OCR* of a hypothetical, normally consolidated, fine grained surficial seabed sediment. Stable, fully-normally consolidated sediments will have an OCR of one and a linearly increasing quasi-static bearing capacity (*qsbc*) with depth. Deposition of additional, unconsolidated, sediments will change the *qsbc*-depth profile but have no effect on OCR. However, erosion of sediment will lead to an OCR of greater than one and values of *qsbc* higher than expected for normally consolidated sediments.

Proceedings of Coastal Sediments 2015, San Diego
Wang, P., Rosati, J.D., and Cheng, J. (Eds.)

Chapter 2. Manuscript 1

In-situ Geotechnical Investigation of a Confined Sediment Disposal Facility: Sydney Harbour, Nova Scotia

Jared Dorvinen[1], Nina Stark[1], Bruce Hatcher[2], Matthew Hatcher[3], Vincent Leys[4], and Achim Kopf[5]

[1]Virginia Tech, Department of Civil and Environmental Engineering, 200 Patton Hall, Blacksburg, VA 24061, USA

[2]Bras d'Or Institute for Ecosystem Research, Cape Breton University, P.O. Box 5300, 1250 Grand Lake Road, Sydney, NS B1P 6L2, Canada

[3]Dalhousie University, Dept. of Oceanography, 1355 Oxford St, Halifax, Nova Scotia, B3H 4R2, Canada

[4]CBCL Limited, 1489 Hollis St, Halifax, Nova Scotia, B3J 3M5, Canada

[5]MARUM, University of Bremen, Leobener Str., 28359 Bremen, Germany

2.1 ABSTRACT

During the winter of 2011-2012, 4.2 million cubic meters of material was dredged from the navigation channel of Sydney Harbour. 3.8 million Cubic meters of this sediment was used to construct a Confined Disposal Facility (CDF) on the western shore of Sydney Harbour's South Arm. In October 2012 and July 2013, two surveys utilizing the free-fall penetrometer *Nimrod* were undertaken to investigate the sediment dynamics of the Harbour and evaluate the stability of recently deposited dredged sediments at the CDF and throughout the channel. The results of these two surveys showed a consistent trend of consolidation of the dredge material and a decrease in the thickness of the potentially mobile sediment top layers. In addition to the marked decrease in the top layer thickness (TLT), slumping of newly deposited dredged sediment from the near-shore, toward the mid-channel, was observed.

2.2 Introduction

Located on the Northern coast of Cape Breton; Sydney Harbour is the second busiest port in the province of Nova Scotia after Halifax (Fig. 2.1). Its waters accommodate four ferries connecting daily with the Canadian island province of Newfoundland, cruise ship visits (∼70 per year), commercial shipping (oil, coal, and cargo), Government vessels (Coast Guard and Navy), a commercial fishing fleet, and many recreational boats (total of 150 small vessels). As commercial cargo vessels continue to grow in size and recreational cruises become more popular, it is important for ports to maintain and expand their facilities in order to remain functional and competitive (McCalla 1999).

In late 2011-2012, major dredging operations were undertaken in order to maintain and expand the Harbour's port facilities. These interventions consisted first of the dredging of 4.2 million cubic meters of sediment from the Harbour's entrance channel, and second, the construction of a Confined Disposal Facility (CDF). Approximately 3.8 million cubic meters of the coarser dredge spoil was used to construct the 74 ha CDF (Stark et al. 2014a). The remainder of the finer dredged sediment was re-suspended in the Harbour waters during dredging.

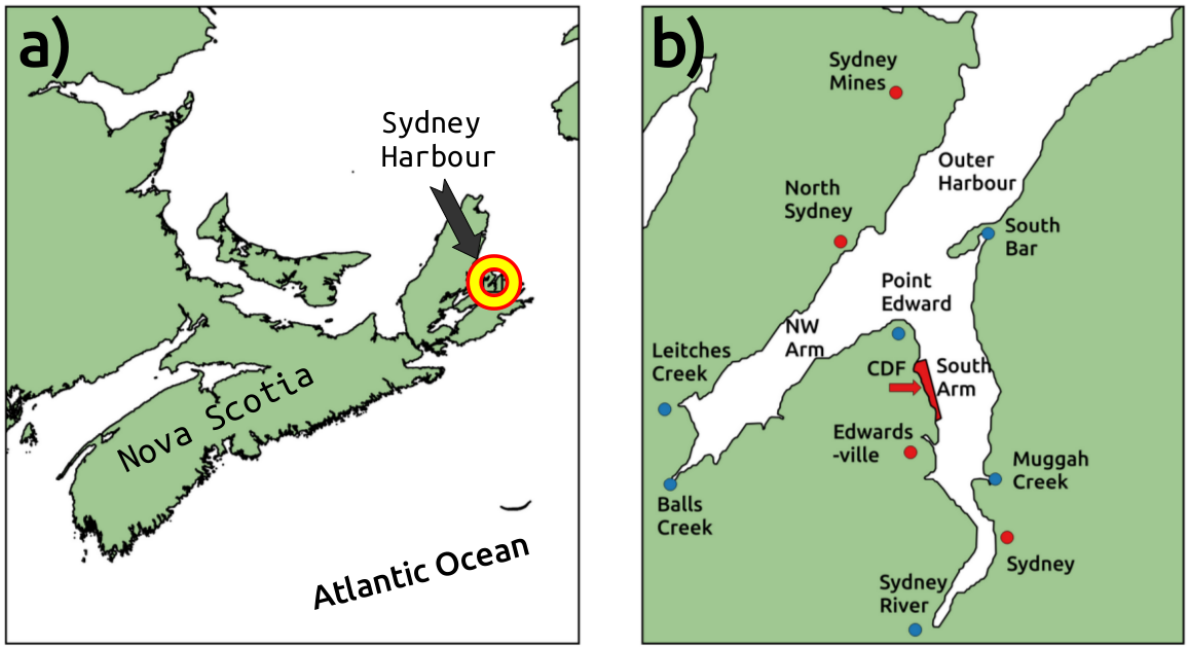

Figure 2.1: Study location overview, a) the location of Sydney Harbour in the province of Nova Scotia, b) a plan view of the Harbour.

Sydney Harbour has low sedimentation rates, 0.2 to 0.8 cm/year (Smith et al. 2009). However, during dredging this rate increased to 26 to 128 cm/year (Walker et al. 2013). During

surveys prior to the dredging of 2011-2012, total suspended solids in the Harbour were found to be less than 10 mg/L, one meter above the sediment- water interface (CBCL 2009a). Sediment composition in the South Arm is mainly silt and clay at $\sim 80\%$ (Jacques Whitford Limited 2009a). Average estimated fresh water inflow to the South Arm is 11.4 m^3/s, 10.2 m^3/s coming from the Sydney River and 1.2 m^3/s from Muggah Creek. Tides in the Harbour are semi-diurnal with a typical tidal range from 0.1 meter to 2.3 meters chart datum (CBCL 2009a). Mean current velocities near the bed in the Harbour are less than 2 cm/s directed up-harbor (CBCL 2009a). The predominant direction of off-shore waves impacting the Harbour is from the north east, while winds are primarily from the south west (CBCL 2009a). Water depths at the channel thalweg ranged from 15 to 20 meters pre-dredging. The channel was dredged to a nominal depth of 17.5 meters (Stark et al. 2014a).

In October 2012, a geotechnical survey of Sydney Harbour was undertaken with the purpose to: (i) map areas of sediment erosion and deposition, (ii) determine the thickness of recently deposited sediments and potentially mobile sediment layers, and (iii) estimate the strength and consolidation state of superficial seafloor sediments in the Harbour. In 2013, a follow up survey was completed to observe changes in these properties with time. The nine months between the two surveys included the winter months in which hydrodynamic conditions in the Harbour are typically the most energetic (CBCL 2009a).

Given the extent of the recent engineering actions in the port of Sydney, important questions related to the sediment dynamics of the Harbour exist: Is the layer of newly deposited dredged material stable and consolidating? Is the bund wall of the newly constructed CDF stable under typical conditions? These questions are important, for reasons related to benthic habitat and water quality, as well as navigation, and are addressed by these two surveys.

2.3 Methods

In-situ geotechnical surveys were carried out in October 2012 and July 2013 to investigate sediment mobility and deposition following the dredging and relocation operations of 2011-12. Both surveys included a sample transect in the northern entrance to the South Arm of the Harbour as well as a transect extending from the new shoreline of the CDF to mid-channel (Fig. 2.4). During these surveys, the portable penetrometer *Nimrod* was deployed from a Zodiac™RHIB for the geotechnical assessment of the uppermost seafloor sediment layers. Sediment grab samples as well as photographs of the penetrometer impact locations were obtained with diver support to augment the penetrometer data. Depth measurements were made using a RayMarine™200 kHz sounder, typical accuracy better than 0.5 m. Depth data were corrected to chart datum using the minute-by-minute tidal record from the North Sydney tide gauge station.

The dynamic free-fall penetrometer, *Nimrod*, is equipped with five on-board MEMS accelerometers, two 3D tilt sensors, internal and external temperature sensors, a pressure

sensor located behind the cone, and a 1 kHz data logger. The use of accelerometers, rated to: $2g$, $18g$, $35g$, $70g$, and $250g$, allows the probe to measure vertical impact decelerations ranging from $0.1g$ to $250g$. First integration of the measured deceleration produces a penetration velocity profile, while a second integration gives penetration depth. The quasi-static bearing capacity (*qsbc*) is estimated using the semi-empirical correlations presented by Stark et al. (2012). Sediment layering can be inferred from the depth-deceleration profile and vertically resolved to $\pm$ 1 cm (Stark and Wever 2009).

When processing data collected using free-fall penetrometers one must first identify impact events in the continuous accelerometer records and then select their start and end points. Mulukutla et al. (2011) observed that while an impact theoretically occurs at a single given point in the data record, this point can be difficult to resolve due to the presence of suspended solids at the mud-line.

However, in addition to a poorly defined sediment-water interface, sensor noise can play an equally large role in obscuring an impact. In this study, a simple method was used to improve the resolution of the point of impact by more fully exploiting the data being collected by the free-fall penetrometer *Nimrod* (Fig. 2.2). Instead of using a single accelerometer to resolve a deployment, two separate accelerometers were used for each impact profile (Fig. 2.2a). First, the $2g$ accelerometer was used to select the initial point of impact and the beginning of damped oscillation as the penetrometer comes to rest (Fig. 2.2b).

The high resolution of this sensor makes this task less ambiguous than when using a higher capacity but lower resolution sensor for the entire impact. Next, a sensor that fully captures the entire impact profile is chosen (Fig. 2.2c). The data from that sensor is then spliced with data from the $2g$ accelerometer to fully capture the impact. This is done by clipping the profiles at a point before the $2g$ accelerometer's sensing capacity is exceeded and then combining the data from the two sensors at this location (Fig. 2.2d). By employing this method very soft and thin top layers can be resolved, even when overlaying a much harder substrate. Once the deceleration profile has been defined, the method presented by Stark et al. (2012) is used to calculate an estimate of *qsbc* with depth for the impact. An illustration of this process follows (Fig. 2.3a-c). The deceleration profile is first integrated to produce a velocity-depth profile (Fig. 2.3a-b). From the velocity- and deceleration- depth profiles a *qsbc*-depth profile is then calculated by applying semi-empirical equations that take into account the changing bearing-area with depth as well as strain-rate effects occurring during an impact event (Fig. 2.3c).

Once all impact profiles were resolved and processed, each deployment location was characterized based on four criteria: maximum penetration, maximum *qsbc*, *qsbc* at 10 cm of penetration, and penetration depth at which *qsbc* exceeds 1 kPa. The *qsbc* at 10 cm of penetration was used as an estimate of surface strength (SS) while the depth at which the *qsbc* exceeds 1 kPa was used as an estimate of soft sediment top layer thickness (TLT). Measured SS can be used to compare how erodible the seabed surface is at different locations, while TLT can be used to estimate the amount of sediment available to be easily eroded. These re-

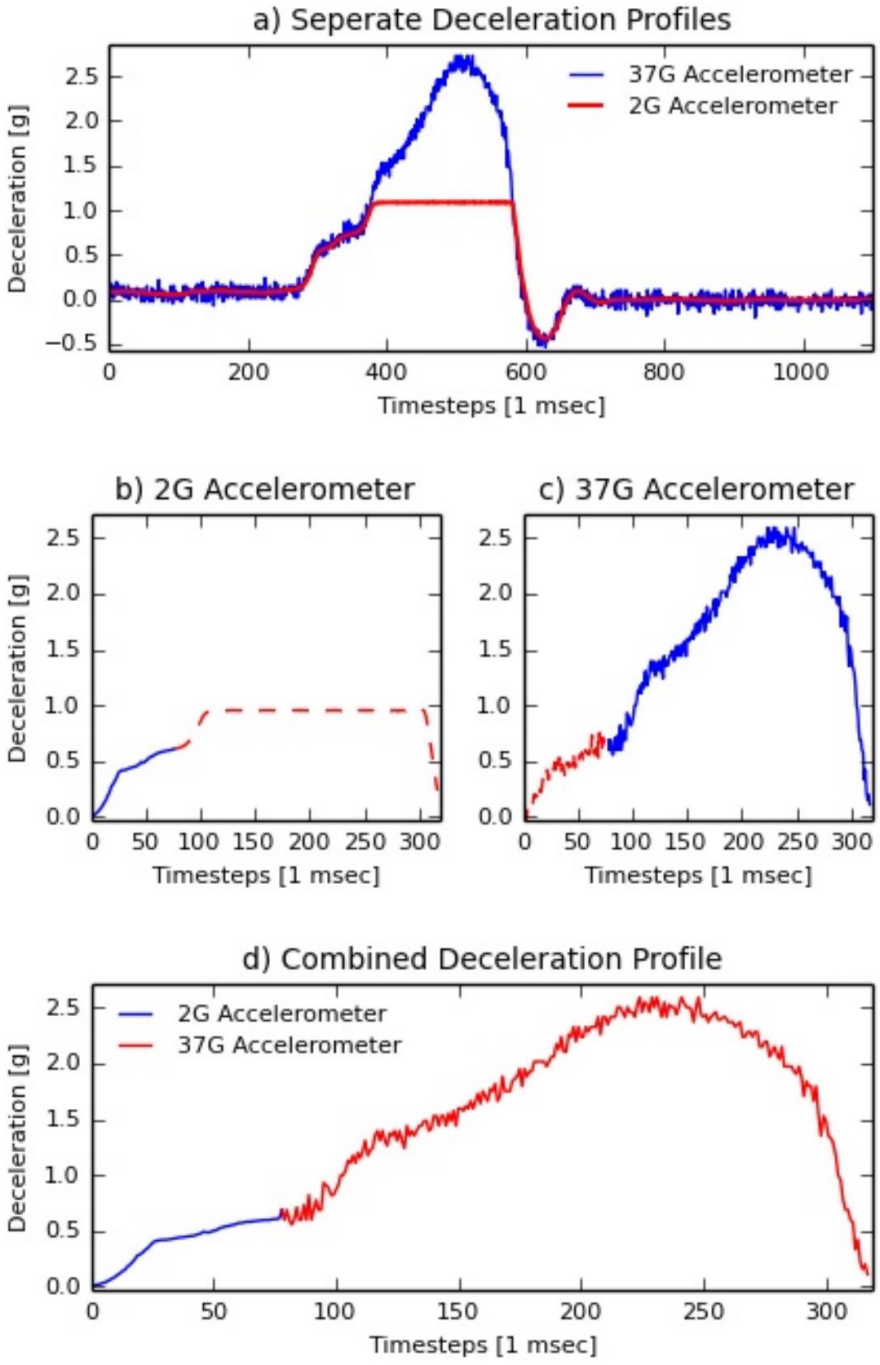

Figure 2.2: An illustration of the two sensor method used for resolving impact profiles

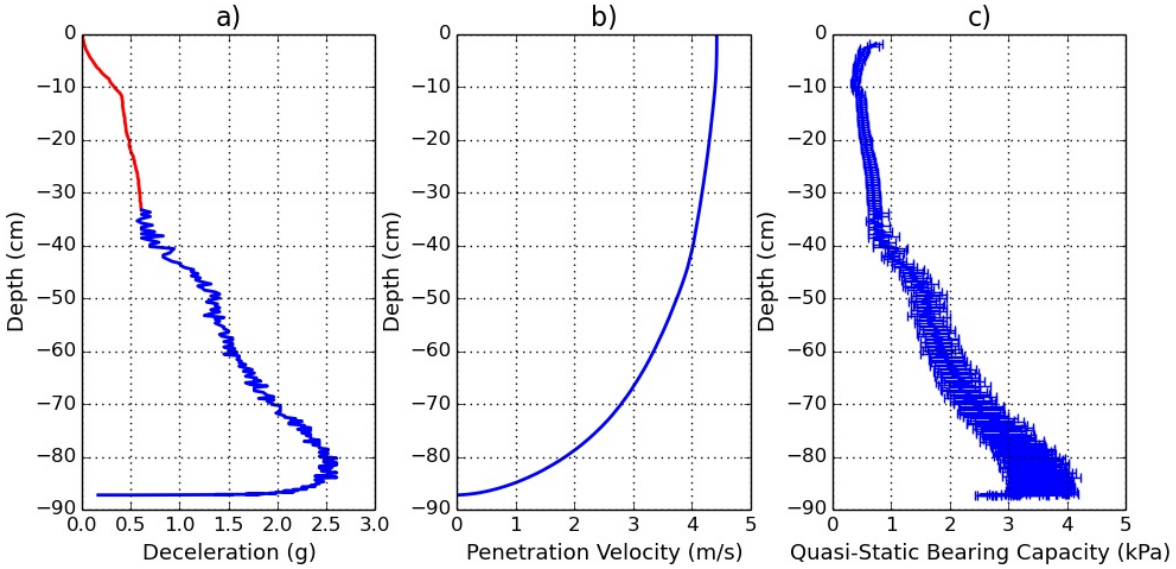

Figure 2.3: Penetrometer results while using the two sensor method. Shown are the results of a typical penetrometer deployment in the mid-channel of Sydney Harbour

sults were plotted Geo-spatially using QGIS Desktop, a Free/Open Source Software (FOSS) geographic information system (Fig. 2.4).

2.4 Results

During the 2012 survey, 208 *Nimrod* deployments at 104 locations were made in the South Arm of Sydney Harbour. In 2013, 33 deployments were completed, each at a distinct location. Water depths at the deployment locations ranged from 1-19 meters in 2012 and from 5-19 meters in 2013. Impact velocities varied from 3.6-5.8 m/s in 2013 and 2.7-6.0 m/s in 2012. While maximum decelerations ranged from $1.3g$ to $210g$ in 2012 and $1.6g$ to $43.2g$ in 2013.

The highest values of *qsbc* and deceleration in 2012 were observed near Edwards Point (26-187 kPa, $22g$ to $155g$) and the CDF (50-400 kPa, $13g$ to $60g$) (Fig. 2.4). In 2013 the highest *qsbc* and deceleration in the South Arm were 86 kPa and $43g$ respectively, observed near the CDF. In 2013, no *Nimrod* deployments were made near Edwards Point and the closest deployment to the CDF was made 58 meters offshore, whereas the previous year's deployments were made as close as 15 meters offshore. In both years' surveys, minimum values of deceleration and *qsbc* ($dec < 4g$, $qsbc < 5$ kPa) were seen near the middle of the channel. The hardest impact locations experienced penetration depths of less than 20 cm while penetration depths of more than 80 cm were observed at the softest locations.

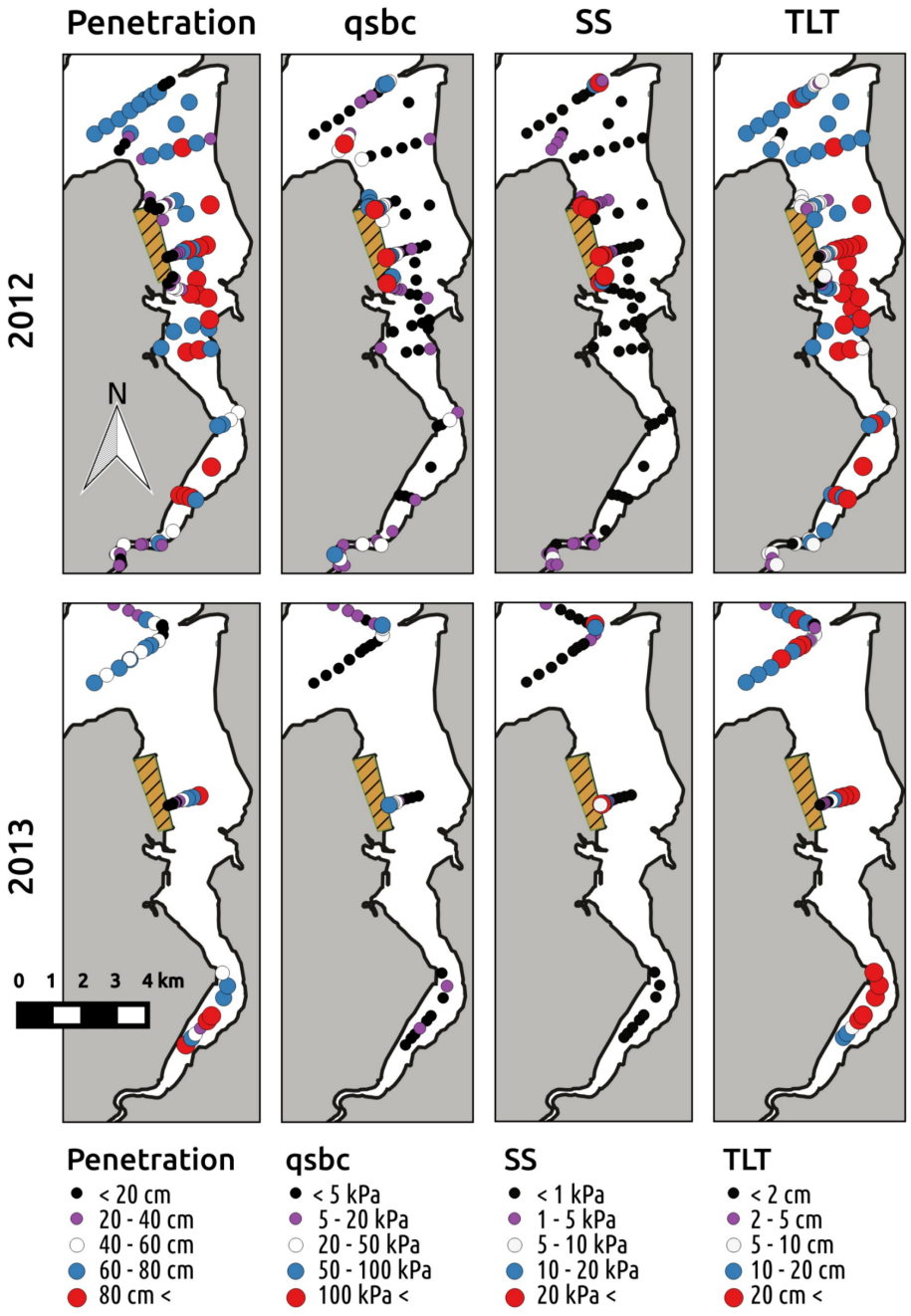

Figure 2.4: Results of the 2012 and 2013 surveys in the South Arm of Sydney Harbour

In 2012, TLT values of 2-105 cm were observed while in the 2013 survey the TLT ranged from 0-45 cm in the South Arm. The largest values of TLT were consistently found toward the center of the channel, while thinner top layers were observed near the shoreline and adjacent to the CDF. Surface strengths (SS) of over 20 kPa were observed near the CDF and South Bar in 2012, similar values of SS were found at these locations in 2013. The large majority of deployment locations in the mid-channel region had SS values of less than 1 kPa in both surveys.

Although the survey in 2013 did not include as many *Nimrod* deployments as the 2012 survey, the two transects in the South Arm which were repeated in both surveys can be directly compared. The first transect, located in the entrance to the South Arm, extends south west from the South Bar across the channel and to the north of Edwards Point. The second transect is located adjacent to the CDF and extends from the near-shore of the CDF eastward into the middle of the channel (Fig. 2.4). Figure 2.5 shows how the observed TLT and water depth changed along these two transects over the nine month survey period.

Along the transect in the entrance to the South Arm, the average depth decreased by 0.4 meters from 2012 to 2013. At the same time, the average observed depth near the CDF decreased by 0.3 meters (Fig. 2.5). The average TLT in the entrance to the South Arm was 18.3 cm in 2012 and had decreased to 15.3 cm by 2012. Likewise, the average TLT near the CDF decreased from 18.0 cm in 2012 to 11.7 cm in 2013.

The dredged channel can be seen clearly at the entrance to the south arm (Fig. 2.5a). It is interesting to note that in the near-shore region of both profiles, slumping is observed between the 2012 and 2013 surveys as the deposited dredged material moves downslope towards the center of the channel. Table 2.1 summarizes the observed changes in all four impact variables in Figure 2.4: maximum penetration, maximum *qsbc*, SS, and TLT. The average *Nimrod* penetration depth was seen to decrease by 8.4 cm in the entrance to the South Arm (SA) and 7.4 cm near the CDF. Likewise, the average maximum *qsbc* decreased by 1.3 kPa and 0.5 kPa along entrance to the SA and near the CDF respectively. Average SS was seen to increase by 0.2 kPa in the entrance to the SA and by 1.2 kPa adjacent to the CDF. TLT decreased 3.0 cm along the SA transect and 6.3 cm near the CDF.

Table 2.1: Summary of *Nimrod* results

(a) Maximum *Nimrod* penetration (cm)

Transect	2012 Mean Pen.	2013 Mean Pen.	Avg. Change
Entrance to S.A.	62.3	53.9	-8.4 (σ=7.2, n=11)
Near CDF	47.1	39.7	-7.4 (σ=6.9, n=11)

(b) Maximum *qsbc* (kPa)

Transect	2012 Mean *qsbc*	2013 Mean *qsbc*	Avg. Change
Entrance to S.A.	7.0	5.7	-1.3 (σ=1.0, n=11)
Near CDF	20.7	20.3	-0.5 (σ=14.3, n=11)

(c) Sediment bearing capacity (kPa) at 10 cm penetration

Transect	2012 Mean SS	2013 Mean SS	Avg. Change
Entrance to S.A.	0.6	0.8	0.2 (σ=0.3, n=11)
Near CDF	6.6	7.8	1.2 (σ=5.4, n=11)

(d) Penetration depth at which sediment bearing capacity exceeds 1 kPa (cm)

Transect	2012 Mean TLT	2013 Mean TLT	Avg. Change
Entrance to S.A.	18.3	15.3	-3.0 (σ=4.6, n=11)
Near CDF	18.0	11.7	-6.3 (σ=4.5, n=11)

2.5 Discussion

2.5.1 Two-Sensor Method

While the two-sensor method employed in this study allowed for improved resolution of penetrometer impacts with the seafloor, data interpretation across the majority of impact sites was nearly the same as accomplished by using a single accelerometer. The greatest difference between the two methods was seen in areas where a very soft top layer was found overlaying

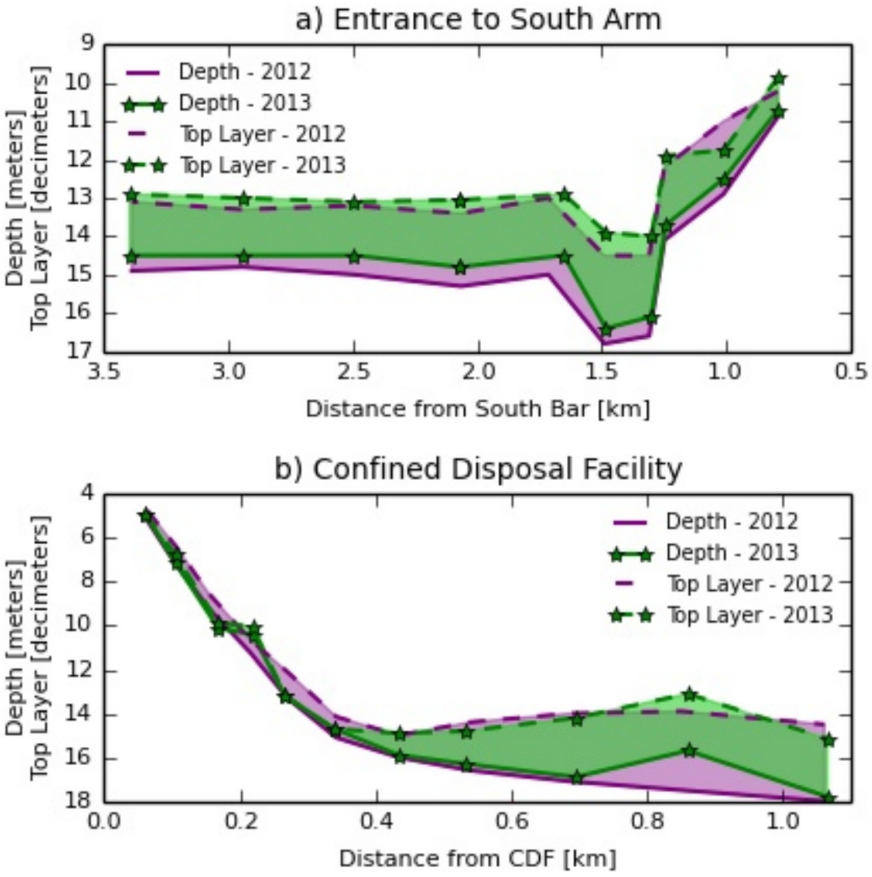

Figure 2.5: TLT and depth moving along transects in the South Arm, shaded regions represent TLT

a harder substrate. In such situations, where the use of a high capacity accelerometer was required to capture the entire impact profile, the noise in the signal of the high capacity sensor obscured the point of impact with any soft top layer. When using a lower capacity and higher resolution sensor the effects of sensor noise are reduced and the resolution of the point of impact is improved.

While using multiple accelerometers was beneficial for increasing the resolution of the initial point of impact with the seabed, there were drawbacks to this method associated with splicing the time series of multiple sensors. Any lag in data-logging experienced by a sensor needs to be corrected before splicing datasets to avoid creating artificial steps in the deceleration profile. Also, if the point at which the two data-series are joined is too close to the maximum capacity of the smaller accelerometer, lag in the sensor response as it nears capacity can cause an artificial break in the deceleration profile. However, the effects of these pitfalls can be easily avoided through basic quality control measures. An example of the successful implementation of this method is shown in Fig. 2.2 and Fig. 2.3.

By examining the deceleration-depth profile in Fig. 2.3a, it is apparent that there exists a distinct break in the changing rate of deceleration at approximately 10 cm of penetration. Likewise, at about 47 cm another break occurs. The first such break at the beginning of the deceleration-depth profile corresponds to the changing bearing-area of the penetrometer's conical tip, as it enters the seabed. While the existence of such an impact signature is no surprise, being cognizant of its presence is nonetheless useful to ensure the best approximation of the moment of impact with the seafloor is made. The second break seen in the profile is an indication that the penetrometer is passing from one distinct layer of sediment to the next. Again, the shape of this break is an artifact of the penetrometers conical tip as much as it is of sediment properties.

2.5.2 Sediment Properties

Inside the South Arm of Sydney Harbour, the layer of loose dredge material deposited in 2011-2012 appears to be stable and consolidating. This is expected given the natural low-energy hydrodynamic environment present in the inner Harbour (Stark et al. 2014a; CBCL 2009a). It is unclear whether wake waves from ship traffic in the Harbour are responsible for the slumping observed in the near-shore bed material, although sediment mobilization and erosion from such wakes are known to occur (Rapaglia et al. 2011). Sediment mobilization in the mid-channel was not observed. This is positive from the benthic habitat and water quality stand points, given the history of sediment contamination in the South Arm of the Harbour, as well as for maintenance and navigation purposes (Smith et al. 2009).

Decreases in penetration depth and TLT, along with an increase in SS suggest that the fine dredged material deposited in the Harbour is consolidating and forming a stable bed-layer. While the recorded decrease in average maximum $qsbc$ may seem counter intuitive, considering the significant decrease in average penetration depth, this shouldn't be the case.

Typically, the maximum *qsbc* experienced by *Nimrod* during a given impact occurs near the end of penetration, (e.g. Fig. 2.3c). As the soft top layer sediments consolidate and gain strength, they provide more resistance to penetration during a *Nimrod* impact. However, in the absence of further significant sediment deposition, this consolidation of the uppermost layer of sediments does nothing to increase the strength of the underlying seabed.

Therefore, if the decrease in penetration depth is greater than the reduction in TLT, the maximum *qsbc* observed at a given location will decrease. Slumping of sediments near the bund wall of the CDF and just off the South Bar in the entrance to the South Arm was observed in the 2013 survey. The average grade in the areas experiencing slumping is at least 0.01, if not greater. The typical critical slope for the initiation of gravity flows of an unconsolidated fluid mud layer is about 0.01 to 0.02 (McAnally et al. 2007). It is then not surprising that the layer of unconsolidated fine dredge material in these areas was mobilized. It is unknown whether or not the hydrodynamic forces associated with ship traffic played a significant role in this process. Further investigation is warranted to see if this slumping continues once the fine dredge material has been transported completely out of these areas.

2.6 Conclusions

Two geotechnical surveys assessed sediment remobilization and deposition 9 and 18 months after dredging and construction of a Confined Disposal Facility in Sydney Harbour. The dynamic penetrometer *Nimrod* was employed to quantify the strength and thickness of superficial sediment layers to track changes in their potential mobility during the survey interval. Additionally, a revised technique for detecting and resolving the first centimeters of impact with the seafloor in a deceleration time-series was successfully employed. There are a couple of conclusions that can be made from the results regarding the sediment dynamics in the South Arm of Sydney Harbour:

1. Along multiple survey transects in the Southern Arm of Sydney Harbour, a trend of consolidation is observed in the uppermost layer of seafloor sediments.

2. Slumping of newly deposited fine dredge material occurred on the bund wall of the CDF as well as off of the point of the South Bar. These areas of the Harbour are characterized by water depths of less than 10 meters and slopes with a greater than 1% grade.

Areas of interest for future surveys and investigations include: continued observations of TLT and SS to see if the trends of consolidation observed here will continue, as well as monitoring the progression, effects, and causes of slumping sediments on the bund wall of the CDF and near the shore of the South Bar.

Chapter 3. Manuscript 2

ESTIMATING *IN-SITU* SEDIMENT CONSOLIDATION STATE USING A FREE-FALL PENETROMETER: SYDNEY HARBOUR, NS

Jared Dorvinen[1], Nina Stark[2], Bruce Hatcher[3], Matthew Hatcher[4], Vincent Leys[5], and Achim Kopf[6]

[1]M.S. Student, Virginia Tech, Department of Civil and Environmental Engineering, 200 Patton Hall, Blacksburg, VA 24061, USA (corresponding author). E-mail: dorvinen@vt.edu

[2]Assistant Professor, Virginia Tech, Department of Civil and Environmental Engineering, 200 Patton Hall, Blacksburg, VA 24061, USA.

[3]Associate Professor, Bras d'Or Institute for Ecosystem Research, Cape Breton University, P.O. Box 5300, 1250 Grand Lake Road, Sydney, NS B1P 6L2, Canada.

[4]Dalhousie University, Dept. of Oceanography, 1355 Oxford St, Halifax, Nova Scotia, B3H 4R2, Canada.

[5]Coastal Engineer, CBCL Limited, 1489 Hollis St, Halifax, Nova Scotia, B3J 3M5, Canada.

[6]Professor, MARUM, University of Bremen, Leobener Str., 28359 Bremen, Germany.

3.1 ABSTRACT

Two *in-situ* geotechnical surveys were undertaken in Sydney Harbour, Nova Scotia following the dredging and relocation of 4.2 million-m^3 of sediment from the shipping channel during the fall and winter of 2011-12. The surveys were conducted nine and eighteen months after dredging using the portable, free-fall penetrometer *Nimrod*. A new method for interpreting the state of sediment consolidation from free-fall penetrometer data was developed and applied to identify areas of sediment erosion and deposition. Results nine months after

dredging showed an initial accumulation of dredge-resuspended sediments, in agreement with the predictions of a sediment deposition model. Eighteen months after dredging stability and evidence of consolidation or continued accumulation was found at $> 92\%$ of the thirty-nine sampled locations examined. Limited erosion was observed at just three locations. The general pattern of sediment stability observed is consistent with the historically-low energy and sedimentation environment of the inner regions of Sydney Harbour.

3.2 Introduction

The maintenance and expansion of port facilities, including dredging of navigation channels, is vitally important for the long term economic viability of a port and is becoming an increasingly relevant issue as ships continue to increase in size (McCalla 1999). Sediment transport processes can reduce the effective water depth of a port by infilling the navigation channel, reducing the utility of the port's facilities if maintenance dredging is not done. Depending on the rate of channel infilling, dredging may be required as frequently as every day in order to maintain navigable water depths (Lund 1990; van Craenenbroeck et al. 1998). In order to avoid the cost of unnecessary dredging while still maintaining full functionality of a port, sediment deposition models are used to optimize dredging schedules and assess the viability of dredging projects (Lund 1990). However the accurate prediction of dredging requirements, based on sedimentation rates and distribution, requires the calibration and validation of modeling results with field data. Proper disposal of dredged material is important to reduce the ecological and economic impacts associated with dredging (USACE 1983). Understanding of the sediment transport regime and distribution patterns at a dredging site allows engineers to plan dredging activities in order to minimize the transport of material back into the dredge channel or into environmentally sensitive areas. This is especially important when dealing with contaminated sediment (USACE 1983).

Dredging in Sydney Harbour (Fig. 3.1a) began in early October of 2011 and lasted until mid-January of 2012. A trailing hopper suction dredge (M.V. *Oranie* Boskalis-Westminster NV) was used to remove approximately 4.2 million-m^3 of sediment from the navigation channel into the commercial shipping port. Of this, 3.8 million-m^3 were relocated to a Confined Disposal Facility (CDF) in the South Arm of the Harbour (orange box in Fig. 3.1a). This process involved the construction of a bund wall perimeter using the coarser fraction of the dredged material surrounding the $\sim$ 58 ha CDF, into which was subsequently pumped the finer, contaminated sediments dredged from the inner Harbour segment of the navigation channel.

The remaining 0.4 million-m^3 of sediment, primarily fine material, was suspended as overwash from the dredge ship while it was operating. It formed a sediment plume that was transported by wind and tide-driven circulation, and settled in patches of fine dredge material, 3-90 cm thick, throughout the Harbour (Walker et al. 2013a; Stark et al. 2014a).

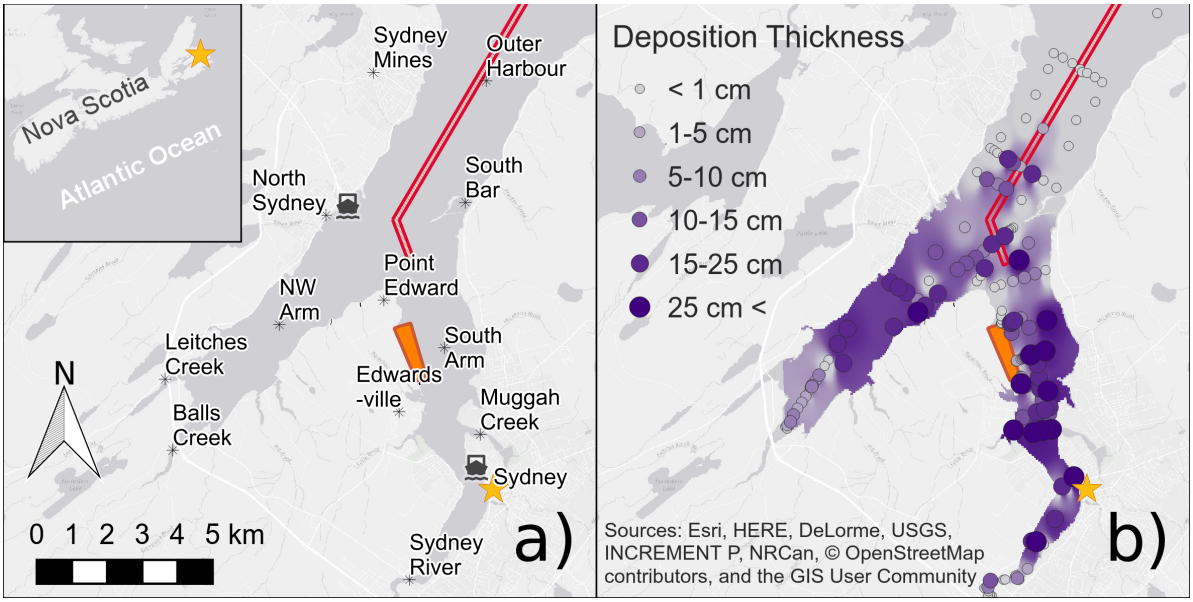

Figure 3.1: Sydney Harbour layout, a) the location of Sydney Harbour in Nova Scotia and points of interest in the Harbour, b) initial distribution of a superficial layer of soft soil following dredging (based on survey results from 2012). The red "hockey stick" shaped box indicates the dredged channel. The orange box shows the location of the Confined Disposal Facility (CDF).

Portable free-fall penetrometers have proven their usefulness as tools for the rapid, *in-situ* geotechnical characterization of surficial seabed sediments (Stoll 2004; Stoll et al. 2007; Stark et al. 2009b, 2014a). By measuring deceleration while penetrating the sea-floor, sediment strength and layering can be inferred, areas of erosion and deposition can be mapped, and dredged material can be located (Stark and Wever 2009; Stark and Kopf 2011; Stark et al. 2014a). Due to the ease of handling and deploying these instruments, this information can be gathered in a rapid and cost effective manner (e.g., 130 deployments over ~ 8 km^2 during a 3 hour survey period on one of the Sydney Harbour survey days in October 2012).

Two *in-situ* geotechnical surveys were conducted using the *Nimrod* penetrometer to understand the deposition behavior and stability of dredged sediment in Sydney Harbour, and its potential impacts; one survey in October 2012 (9 months after the completion of dredging), and the other in July 2013. The survey in October 2012 identified three major dredged material deposition zones: one in the area surrounding the CDF in the South Arm of the Harbour, a second at the junction of the three main arms of the Harbour, and a third in the Northwest Arm of the Harbour near the outflow of Balls Creek (Fig. 3.1b). This distribution of dredged material deposition aligned closely with the results of a dredge plume deposition model produced by CBCL Limited prior to dredging (CBCL 2009b; Stark et al. 2014a). However, the thickness of dredge sediment layers in parts of the Harbour (Northwest Arm

junction) was observed to be larger (up to 20 cm) than model predictions indicated (Stark et al. 2014a). The second survey in July 2013 aimed to determine the fate of the dredge-resuspended material and seabed sediments after an additional nine months had passed since the completion of dredging. Three questions were addressed: Is the spatial distribution of the dredge material stable? In what areas of the Harbour is sediment accumulating, eroding, or neither? What are the economic/ecological implications of the ongoing sediment dynamics in Sydney Harbour? The following sections detail the physical setting of Sydney Harbour, the methods used during surveying and data processing, results, a discussion of the results and methods in the context of current literature, and conclusions about the questions posed.

3.3 Physical Setting

Sydney Harbour is located on the northern coast of Cape Breton in the Atlantic Canadian province of Nova Scotia (Fig. 3.1a). It is a bifurcated estuary covering an area of ~ 52 km^2. Its port facilities represent the eastern-most terminus of the Trans-Canadian Railway, and the first mainland deep-water port available to ships crossing the Atlantic from Central and Northern Europe. Due to this location, Sydney Harbour is also a main access point for goods and passengers traveling to and from the Canadian island of Newfoundland, with ferries running 2-5 times daily. In addition to the port's importance as a shipping and passenger hub for the region, it also receives approximately 70 cruise vessels annually, and supports a lobster fishery comprising more than forty vessels. This combination of commercial maritime activities, plus the coast guard and recreational boating sector, creates a dynamic port environment (Gregory 1993).

The Harbour has the shape of an inverted 'Y' with its primary axis extending approximately 16 km northeast to southwest from the open seaward mouth of the Harbour, to the inflow of the Sydney River at the inland end of the South Arm (Fig. 1a). The width of the Harbour ranges from about 3 km at the mouth to just over 1.5 km near the CDF (South Arm). Surface sediments in and around Sydney Harbour consist largely of glacial till, with underlying Carboniferous era sedimentary deposits (Jacques Whitford Limited 2009b). Sediment grain sizes in the Harbour range from mainly silt/clay in the South and Northwest Arms to primarily sand with some gravel in the Outer Harbour (Lee et al. 2002). Typical sedimentation rates near the mouth of Muggah Creek (South Arm) range from 0.2 to 2.0 cm/yr (Stewart et al. 2001; Lee et al. 2002). During dredging in 2011-2012, sedimentation rates of 26 cm/yr up to 128 cm/yr were observed at nearby sites (Walker et al. 2013a).

Meteorological data and historical climate data were obtained from Environment Canada's online records (http://weather.gc.ca/city/pages/ns-31_metric_e.html). A met station located at the Sydney Regional Airport (Latitude: 46.16, Longitude: -60.04) reports wind, temperature, and precipitation data on an hourly basis. Although there were no direct measurements of waves in Sydney Harbour during the study period, modeled wind and wave data were

available for Sydney Bight from the Environment Canada MSC50 Wind and Wave Hindcast (http://www.oceanweather.net/MSC50WaveAtlas/). Hindcast data were extracted for grid point M6010137 (Latitude: 46.28, Longitude: -60.17) over the period from October 1st, 2012 to July 31st, 2013. Water level data were obtained from the Fisheries and Oceans Canada tide gauge in North Sydney (Tide Gauge #: 612, Latitude: 46.21, Longitude: -60.24).

The one-year return period offshore significant wave height (H_s) in Sydney Bight near the mouth of Sydney Harbour is 4.8 m, with a wave period of 10.5 s. A SWAN (Booij et al. 1996) model run with these input wave parameters and a seasonal average northerly wind velocity of 22 m/s produced a H_s of 1.4 m with a period of 4 s near the location of the CDF (CBCL 2009a). The average offshore H_s during the period between the two sediment surveys was 1.03 m, with a maximum hourly-average of 4.67 m occurring on February 9th 2013 (close to the one-year return value). During September 2012, the average and maximum offshore H_s were 0.90 m and 2.82 m (resp.), while the month prior to the second survey in July 2013 experienced average and maximum offshore H_s of 0.41 m and 1.28 m, respectively.

Sydney Harbour is a tidally dominated estuary. Tides are diurnal with mean- and spring-tidal ranges of 0.9 m and 1.4 m (Gregory et al. 1993; CBCL 2009a). Tidal currents have mean velocities of 0.03 m/s, and peak velocities of 0.05 m/s, although seiche-induced velocities of 0.13 m/s have been observed (Gregory et al. 1993; Petrie et al. 2001). None of the tributaries flowing into Sydney Harbour are currently gauged. However, there are various gauged streams throughout Cape Breton. Petrie et al. (2001) used a stream flow dataset from the Salmon River at Salmon River Bridge (Station #: 01FJ001, Latitude: 45.93, Longitude: -60.30, Drainage Area: 199 km^2) to estimate the flow into the South Arm of Sydney Harbour, but this gauging station is no longer operational. Currently, the closest functional gauging station to Sydney Harbour is at MacAskills Brook near Birch Grove, which has recorded both water level and flow rate continuously since 2011 (Station #: 01FJ002, Latitude: 46.12, Longitude: -60.00, Drainage Area: 17.2 km^2). Freshwater inflow to Sydney Harbour was estimated to be proportional to the flow at MacAskills Brook based on the ratio of their contributing watersheds (490 km^2 / 17.2 km^2).

The total recorded precipitation from October 1st 2012 to July 20th 2013 was 1192 mm. This is 106 mm less than the historic average. During the month prior to the first survey (September 1st to 30th 2012), there was a total of 291 mm of precipitation recorded, while for the month prior to the second survey (June 19th to July 18th 2013) precipitation totaled 62 mm. The average freshwater inflow to Sydney Harbour during the nine-month study was estimated to be 18.1 m^3/s, with maximum daily-average inflow of 133.1 m^3/s occurring on June 15th 2013. For the month prior to the first survey the average estimated inflow was 38.1 m^3/s, with a one-day maximum of 128 m^3/s occurring on September 14th. During the month prior to the second survey the mean estimated freshwater inflow to the Harbour was 5.6 m^3/s, with a maximum flow event of 18.0 m^3/s occurring on June 30th. Average flow velocities near the water surface are directed out of the Harbour while near bottom velocities and net bed-load transport are directed upstream, which is typical of an estuarine circulation pattern (Petrie et al. 2001). Average estimated freshwater inflows ranged from 8.5 m^3/s in

July to 38.0 m^3/s in April, with an average of 22.8 m^3/s (Gregory et al. 1993).

During the period between the two surveys in this study, October 2012 to July 2013, meteorological and hydrodynamic conditions were found to be near or below the average conditions for the recorded period of 1981 to 2010. However, conditions during the month prior to the first survey featured greater freshwater inflows and more energetic hydrodynamic conditions than during the month leading up to the second survey in July 2013.

A steel manufacturing facility located near the South Arm of Sydney Harbour operated from 1901 to 1988 (Lambert and Lane 2004). Release of waste effluent from this facility into Muggah Creek (Fig. 3.1a) led to contamination of water and sediment throughout Sydney Harbour (CBCL 1999; Furinsky 2002; Lee et al. 2002; Smith et al. 2009). By 1982, elevated levels of polycyclic aromatic hydrocarbons (PAHs), polychlorinated biphenyls (PCBs), and heavy metals had become so severe that it resulted in the closing of the lobster fishery as a public health concern (Uthe and Musial 1981; Smith et al. 2009). Since the closing of the steel plant in 1988, levels of contaminants in the Harbour's water have been declining as natural sedimentation has capped contaminated sediments, separating them from the water column (Lee et al. 2002; Smith et al. 2009; Walker et al. 2013a). In addition to the recovery through natural processes, *in-situ* stabilization of contaminated sediments at Muggah Creek in 2009 was completed as part of remediation efforts (Walker et al. 2013b). If the material deposited in the Harbour as a result of dredging remains stable, it may augment the natural sedimentation processes and remediation efforts already taking place, further reducing levels of contamination in the Harbour waters and biota.

3.4 Methods

3.4.1 *In-situ* Measurements

Surveys were carried out in October 2012 and July 2013 to investigate the spatial pattern of sediment deposition, the magnitudes of sediment deposition and erosion, and the stability of dredge material following the completion of dredging and relocation operation in January of 2012. The survey design consisted of a series of linear transects extending from the nearshore to the center of the dredged channel, along the axis of the dredged channel, and along the axis of the anticipated trajectory of bed-load transport as predicted by the numerical model (Fig. 3.2a). *Nimrod* was deployed at regular intervals from a rigid hull inflatable boat (Zodiac™SMRN 600) as it proceeded along these transects. The results of the first survey were used to create the sampling design of the second survey, such that effort was spent determining the locations of the geographical boundaries of the recently deposited or transported sediments. *Nimrod* deployments were made at 173 locations in 2012 and 56 locations in 2013 to assess the geotechnical properties of the uppermost seabed sediment layers. Deployments were made during both surveys at 39 of these locations (Fig. 3.2a).

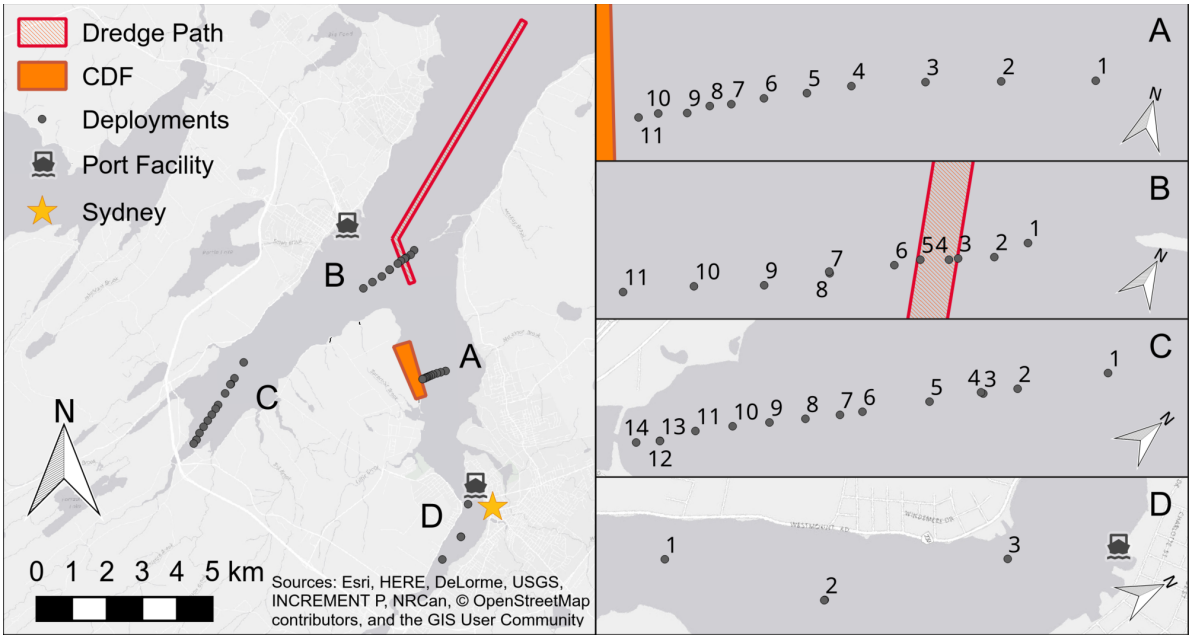

Figure 3.2: *Nimrod* deployments, a) the locations of selected transects in Sydney Harbour along with, b) locations of individual *Nimrod* deployments along each transect. Only those locations surveyed in both 2012 and 2013 are shown.

SCUBA divers collected sediment samples (push cores and grab-samples), and took photographs at 11 of the impact locations in 2013 to augment the penetrometer data. Water depth measurements were made using a RayMarine™200 kHz sounder, typical accuracies better than 0.5 m. The coordinates of each deployment location were recorded using a Garmin Map76 (WAAS enabled) GPS, typical accuracy better than 3 m. Due to vessel drift and GPS uncertainty, these coordinates have a spatial uncertainty of 3 to 10 m for each location depending on the depth of the deployment.

3.4.2 Data Processing

Nimrod is equipped with five on-board micro-electro-mechanical systems (MEMS) accelerometers, two MEMS 3D tilt sensors, internal and external temperature sensors, a pressure sensor located behind the cone, and a 1 kHz data-logger. The use of accelerometers, rated to: $\pm 1.7g$, $\pm 18g$, $\pm 35g$, $\pm 70g$, and $\pm 250g$ (with g being gravitational acceleration), allows the probe to measure vertical impact decelerations ranging from $0.1g$ to $250g$. Data from these sensors can be used to infer strength and layering of surficial sediments (Stark and Kopf 2011; Stark et al. 2012).

Prior to interpretation, several steps must be performed in order to process data from *Nimrod*

deployments. One important step is the identification of the impact events in the continuous accelerometer records, and the selection of their start and end points. Mulukutla et al. (2011) observed that while an impact ideally occurs at a single point in the data record, this point can be difficult to resolve due to the presence of a high concentration of suspended solids at the mud-line. Additionally, sensor noise can play an equally large role in obscuring an impact signature. In order to mitigate this effect, a method for defining seabed impacts by combining the deceleration profiles from two accelerometers was used (Dorvinen et al. 2015). In this method one accelerometer is chosen that satisfies the range of the maximum deceleration reached during the impact, while the second accelerometer chosen is of limited range ($\pm 1.7g$) but higher accuracy to improve resolution at the mud line.

Once the impact profile has been defined the rest of the data processing follows the same method previously described by Stark et al. (2012). First integration of the deceleration profile produces the penetration velocity, and a second integration gives penetration depth. An equivalent of quasi-static bearing capacity (*qsbc*) is estimated using semi-empirical correlations which account for the buoyant weight of *Nimrod*, bearing area, and strain rate effects (Stark et al. 2012). Sediment layering can be inferred from the depth-deceleration profile as well as the *qsbc* profiles, and can be vertically resolved to ± 1 cm (Stoll and Akal 1999; Stark et al. 2009b; Stark and Kopf 2011).

Once the impact profiles were resolved and processed, each deployment location was characterized based on four criteria: maximum penetration depth, maximum *qsbc*, penetration depth to 1 kPa (PD1), and surface strength (TS). Here, we define PD1 as the penetration depth at which the *qsbc* exceeds 1 kPa, and TS as the *qsbc* observed at 10 cm of penetration. The changes in these parameters between the two surveys were quantified, and used to characterize the sediment processes taking place at each location.

3.4.3 Laboratory Tests

Eleven sediment cores and grab samples from 2013 were characterized according to the United Soil Classification System (ASTM D2487-11). Sediment grain-size distribution was evaluated through a combination of sieve and hydrometer testing (ASTM D422). The liquid limit of selected samples was also found using a standard Casagrande cup following ASTM D4318-10e1.

One-dimensional consolidation (oedometer) tests were performed on four of the samples with a load increment ratio (LIR) of 1. Loads started at 2.4 kPa and increased to 2450 kPa over the course of eleven days and were then decreased to 9.6 kPa by quartering daily for four additional days, with each test running for a total of 15 days (ASTM D2435/D2435M-11). The void ratio, e, was calculated at each load increment and plotted versus the consolidation pressure on a logarithmic scale. From the plots of void ratio vs. consolidation pressure, the void ratio at a consolidation pressure of 1 kPa, e_{1kPa}, and the compression index, C_c, were derived. Samples used for oedometer testing were disturbed and reformed at a water content

between 135% and 145% of their liquid limit. This was done to examine their consolidation behavior at water contents similar to those of recently deposited dredged material. It has been suggested that the zero effective stress water content (w_{00}) of a fine grained marine material is a function of a sediment's liquid limit (LL) (Morris 2007). Two proposed relationships include $w_{00} = 4.5LL$ and $w_{00} = 7LL$ (Monte and Krizek 1976; Carrier et al. 1983). These relationships suggest much higher water contents than those tested here. However, due the difficulty of forming samples for oedometer testing at such high water contents, lower water contents were used. Similar water contents have been used for consolidation testing of dredged material by previous authors (e.g. Ju et al. 2003).

3.4.4 Erosion/Deposition Differentiation

Upon impacting the seafloor a cone penetrometer encounters a sediment resistance force, F_{sr}, described in Eq. 1. This force is proportional to the bearing capacity of the soil, q_u, as well as the area of the horizontal plane subjected to the load, A, allowing the assumption that the effects of drag, soil buoyancy, side friction, and adhesion are negligible (Aubeny and Shi 2006; Stark et al. 2012).

$$F_{sr} = q_u * A \tag{3.1}$$

The ultimate bearing capacity of a given soil, q_u, is a function of the cohesion, q_c, surcharge, q_q, and unit weight, q_γ, of the soil at failure as described in Eq. 2 (Terzaghi 1943),

$$q_u = q_c + q_q + q_\gamma = cN_c + {\sigma_{vo}}'N_q + \frac{1}{2}\gamma BN_\gamma \tag{3.2}$$

where c is the sediment cohesion, ${\sigma_{vo}}'$ is the vertical effective stress due to overburden, γ is the unit weight of the soil, B is the characteristic diameter of the penetrating object, and N are bearing capacity factors which account for the effective angle of internal friction, ϕ'. For undrained conditions, such as those encountered during a rapid penetrometer impact into fine-grained soils, N_q and N_γ are equal to 1 and 0, respectively (Terzaghi 1943). In this case, the Mohr-Coulomb failure criteria simplifies to $\tau_f = s_u = c$, and Eq. 2 simplifies to Eq. 3 (Skempton 1951; Stoll 2004).

$$q_u = s_u N_c + {\sigma_{vo}}' \tag{3.3}$$

Stoll (2004) suggests $N_c = 10$ to 15 in undrained cohesive sediment. The ratio of undrained shear strength to vertical effective stress for normally consolidated sediments is known as the undrained strength ratio, *USR*. This ratio (Eq. 4) is typically considered to be approximately constant for a given soil (Mesri 1989; Robertson and Campanella 1983).

$$USR \equiv \frac{s_u}{\sigma_{vo}{}'} \tag{3.4}$$

By rearranging Eq. 4 and then substituting into Eq. 3 we find that the ultimate bearing capacity, q_u, of a normally consolidated cohesive soil is a function of the vertical effective stress $\sigma_{vo}{}'$, the undrained strength ratio *USR*, and the cone factor N_c, as described in Eq. 5.

$$q_u = \sigma_{vo}{}' * USR * N_c + \sigma_{vo}{}' = \sigma_{vo}{}'(1 + USR * N_c) \tag{3.5}$$

Allowing for the assumption that N_c and *USR* are approximately constants for an individual deployment in a homogeneous material, Eq. 5 can be further simplified leading to Eq. 6,

$$q_u = \sigma_{vo}{}'K \tag{3.6}$$

where $K = 1 + USR * N_c$ is a constant for a given soil. In the case of over-consolidated sediments, the shear strength will be higher than would be expected from the normally consolidated *USR* (Hvorslev 1961 pp.9). Therefore, for the over-consolidated case Eq. 6 must be expressed as:

$$q_u \geq \sigma_{vo}{}'K \tag{3.7}$$

Numerous empirical correlations exist for determining the *USR* of a soil based on index properties. Robertson and Campanella (1983) proposed,

$$USR \approx 0.11 + 0.0037 I_w \tag{3.8}$$

where I_w is the plasticity index. Stoll (2004) suggested a range of 10 to 15 for N_c. While knowing the exact values of these parameters would be convenient, these estimates will enable a first order analysis to calculate a reasonable range of values for K. This results in a minimum value of $K \approx 2.1$ for sediments with no plasticity and an N_c of 10, to $K \approx 8.2$ for sediments with an extremely high plasticity index of 100 and an N_c of 15. Sediments in Sydney Harbour are typically silts, silty-clays, or clays of low plasticity. Therefore, a maximum value of $K = 4.3$ results from using an N_c of 15 and a maximum plasticity index of 30 (Skempton 1970). Thus, for normally consolidated, fine-grained sediments encountered in Sydney Harbour, the bearing capacity should be no more than approximately 4.3 times the vertical effective stress.

If the consolidation behavior of a cohesive sediment is known, the ultimate vertical effective stress at any depth in a normally self-weight consolidated layer of that sediment can then be calculated. This value can be used to estimate the upper value of *qsbc* anywhere along the *qsbc*-depth profile for normally consolidated sediment of this type. This means Eq. 6 and

Eq. 7 can be used to compare penetrometer data to idealized, fully consolidated sediments, and distinguish between impact profiles that are likely still consolidating, fully consolidated, or over-consolidated.

If normally consolidated sediments are eroded, the relative consolidation state of the exposed substratum will exceed the theoretical expectations for the respective sediment depth, potentially appearing over-consolidated. Then, following Eq. 7, the bearing capacity, q_u, of the exposed sediment will also be relatively high with regard to the depth of penetration. Relatively high values of TS and a decrease in DP1 would follow. These two parameters can then be utilized as indicators for areas of sediment erosion. In areas of newly accumulating sediment, if sediment is deposited at a sufficiently slow rate, excess pore pressures will not develop, and the strength of sediments at the surface will remain approximately constant over time. However, if sediment is accumulating faster than pore water is able to escape, positive excess pore-pressures will develop, leading to a decrease in the effective stress experienced by sediments near the seabed surface, thereby causing an increase in DP1 while TS decreases or remains constant. In the case of rapid deposition of large amounts of fine sediment, the total vertical stress will increase proportionally to the additional overburden as material is buried. The vertical effective stress (and likewise bearing capacity), however, will remain largely constant over the depth of the newly deposited sediment, as the additional load is offset by an equivalent increase in pore pressure (Skempton 1970). The decision process used to interpret surficial sediment consolidation state from the parameters TS and DP1 is further described in Tab. 1.

Table 3.1: Decision process used to infer sediment consolidation state from penetrometer data

Value of TS	DP1	Sediment Consolidation
TS > predicted range	DP1 < predicted range	over-consolidated (OC)
	DP1 = predicted range	likely over-consolidated
	DP1 > predicted range	soil is non-homogeneous
TS = predicted range	DP1 < predicted range	likely over-consolidated
	DP1 = predicted range	normally consolidated (NC)
	DP1 > predicted range	soil is non-homogeneous
TS < predicted range	DP1 < predicted range	consolidating loose material on OC substrate
	DP1 = predicted range	consolidating
	DP1 > predicted range	consolidating

Note: TS, or toplayer strength, is defined as the *qsbc* at 10 cm of penetrometer penetration. DP1 is defined as the peneration depth at which a *qsbc* of 1 kPa is reached. OC, or over-consolidation ratio, is the ratio of the maximum vertical effective stress experienced by a soil sample over the current vertical effective stress.

3.5 Results

3.5.1 Grain-Size & Classification

The mass-median diameter grain-size, d_{50}, of sediment samples ranged from a low of 3 µm at location D03 in the mouth of the Sydney River in the South Arm, to a high of 121 µm at location A07 near the CDF with an overall average of 45 µm (Fig. 3.2a, Tab. 3.2). Of the six samples that were classified according to the USCS, three were SM Silty Sands, one was a ML Sandy Silt, one was a ML Silt, and one was a MH Elastic Silt (Tab. 3.2). Sediments with sand fractions above $\sim 20\%$ were found at locations near-shore and along seabed slopes on transects A, B, and C, with the one notable exception being location C03 in the middle of the Northwest Arm of the Harbour (Fig. 2b). The large sand content at this location, as well as diver-taken photographs, suggest that this is an area of sediment transport. Otherwise a higher silt/clay fraction would be expected from ongoing natural sediment deposition.

Table 3.2: A summary of laboratory soil testing, specifically results from grain-size analysis, soil classification, and consolidation testing are shown.

Sample	Gravel (%)	Sand (%)	Silt (%)	Clay (%)	d_{50} (µm)	Liquid Limit (%)	C_c -	Void Ratio ($\sigma_v^{'} = 1kPa$)	USCS Classification
A01	0.0	10.6	73.1	16.3	13	-	-	-	-
A07	3.6	72.4	18.0	9.6	121	-	-	-	SM Silty Sand
A09	0.0	52.4	35.0	9.1	99	25.5	0.162	1.00	SM Silty Sand
B02	0.0	34.2	55.0	10.8	36	33.0	-	-	ML Sandy Silt
B08	0.0	5.6	80.9	13.5	13	47.0	0.292	1.56	ML Silt
B11	0.0	5.7	80.0	14.3	14	-	-	-	-
C02	0.0	6.6	77.6	15.8	16	-	-	-	-
C03	6.8	45.4	37.3	9.5	85	37.5	0.207	1.18	SM Silty Sand
C06	3.0	12.5	70.6	13.9	22	62.0	0.380	1.94	MH Elastic Silt
C13	1.9	45.7	42.6	9.8	69	-	-	-	-
D03	0.0	1.4	51.6	47.0	3	-	-	-	-

Note: C_c is the compression index, d_{50} is the mass-median diameter grain-size, and USCS stands for the United Soil Classification System. In the USCS, *SM* means a sand-silt mixture with $> 12\%$ fines, *ML* is an inorganic silt with a liquid limit $< 50\%$ and more than 50% by mass fines, and *MH* is an inorganic silt with a liquid limit and percent fines by mass both $\geq$ 50%.

3.5.2 Oedometer Tests

Oedometer tests were performed on sediment samples from deployment locations A09, B08, C03, and C06. The average void ratio at 1 kPa, e_{1kPa}, and compression index, C_c, for

the four samples tested were found to be $e_{1kPa} = 1.44$ and $C_c = 0.275$ respectively (Fig. 3a). For these four samples, the values of C_c and e_{1kPa} were found to increase and decrease according to the liguid limit of the sediment (Fig. 3b). The sample with the highest liquid limit (LL), and clay content, was extracted from location C06 and had values of $C_c = 0.380$ and $e_{1kPa} = 1.94$. Location A09, which had the highest sand content and lowest clay content of the four samples tested had the lowest values of C_c and e_{1kPa}, 0.162 and 1.00 respectively (Tab. 3.2). Following the analysis presented in the *Erosion/Deposition Differentiation* section and assuming a range of K values from 2 to 4.3, these values of e_{1kPa} and C_c corresponded to predicted TS values for fully normally consolidated sediments in a range of 1 - 3.3 kPa, with higher values expected in areas with sandy sediment and lower values in areas with higher clay contents. This means that in areas with *in-situ* values of TS < 1 kPa, the sediment is likely still consolidating, and in areas with values of TS > 3.3 kPa, erosion is likely occurring or has occurred. In areas where TS is within the predicted range, the sediment can be assumed to be close to fully normally consolidated.

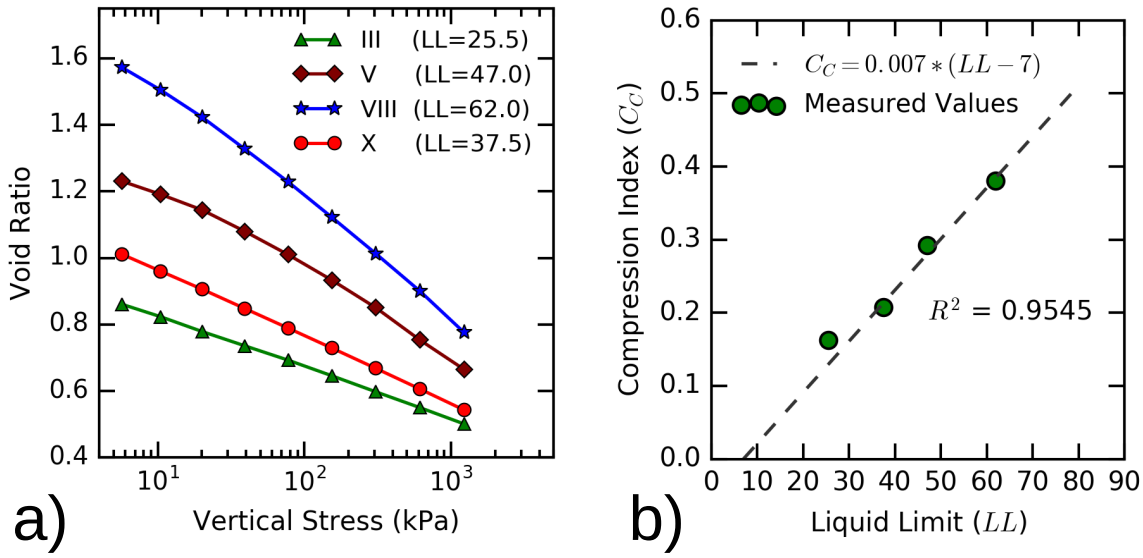

Figure 3.3: Results of oedometer tests, a) compression curves are shown (load increased from 2.4 kPa to 2450 kPa) while the rebound curves (load decreased from 2450 kPa to 9.6 kPa) are omitted as they were unused in this work, b) obtained values of C_c and LL for these samples closely match the empirical relationship proposed by Skempton (1970).

3.5.3 *Nimrod* Surveys

Two spatially distinct trends can be observed in the penetrometer data along *Transect A* from the bottom of the channel in the South Arm to the shore of the CDF (Fig. 3.4).

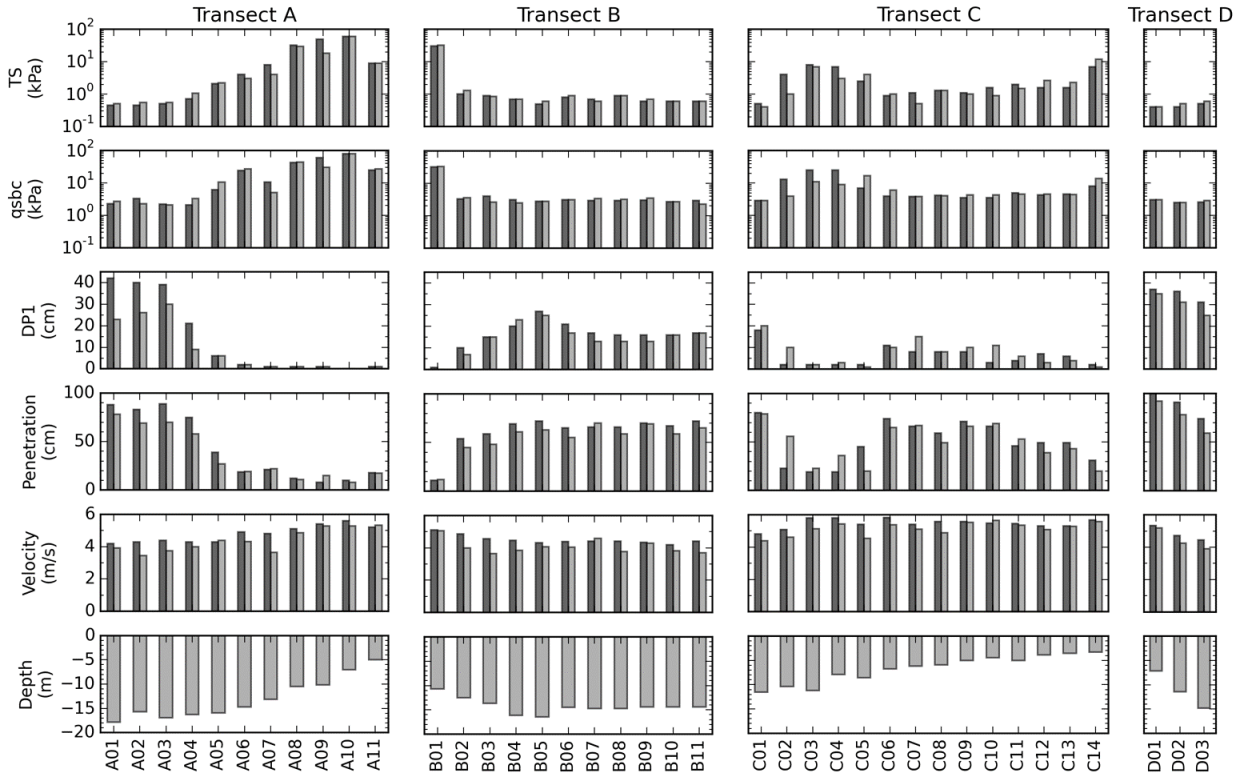

Figure 3.4: Summary of *Nimrod* results from the two surveys of Sydney Harbour. Dark grey bars on the left indicate data from October 2012 while light grey bars on the right represent data from the July 2013 survey.

At locations A01-A05 a trend of slightly increasing TS, decreasing DP1, and decreasing penetration depth over time indicated stability and slight consolidation. From location A06 to A10, TS and *qsbc* increased. This along with increasingly shallow penetrations and low DP1's reflected a transition from soft mud in the center of the channel to the sandy, dredged material comprising the CDF. The generally high values of TS, above the projected maximum value of 3.3 kPa, and *qsbc* at locations A08, A09, A10, and A11 suggested past and, or ongoing erosion at these locations (Fig. 3.4a). The predominantly sandy composition of this material is also likely a factor as the assumptions regarding cohesive sediments and undrained conditions may not hold in these locations. However, the fact that little change was observed between the two surveys indicates sediment stability here, and suggests that this area underwent no to minor sediment transport processes.

Sediment stability and consolidation were found along most of *Transect B* from the South Bar across the dredged channel at the confluence of the three arms of the Harbour (Fig. 3.4b). At locations B02 through B11, low *qsbc*'s and values of TS were consistent with the predominantly normally consolidated, fine-grained material expected here (d_{50} = 13 µm to 36 µm,

see Tab. 3.2). The noticeably higher values of DP1 at locations B04, B05, and B06 coincided with the dredged channel and indicated a greater accumulation of loose, fine material at those locations.

Decreases in DP1 at B02, B05, B06, B07, B08, and B09 over time indicated potential consolidation at these locations, with the remainder of the deployment locations appearing largely stable. Located closest to shore, the high *qsbc* and TS noted at B01 were indicative of predominantly sandy and potentially eroding sediments in this location near the extensive sand bar.

Extending from the southern end of the Northwest Arm of the Harbour approximately 2.8 km to the north-east, *Transect C* is the longest of the four tested transects (Fig. 3.2). Locations C01, C07, and C09 to C11 appeared to be accumulating sediment between the two surveys, as inferred from decreasing TS and increasing DP1 (Fig. 3.4c). Normally consolidated sediments at C05 and over-consolidated sediments at C14 observed during the first survey showed increased TS and decreased DP1 in the second survey. These changes were significant enough to suggest erosion had occured at these locations (Fig. 3.5). The remaining seven deployment locations along *Transect C* appeared to be either consolidating or unchanged between the two surveys.

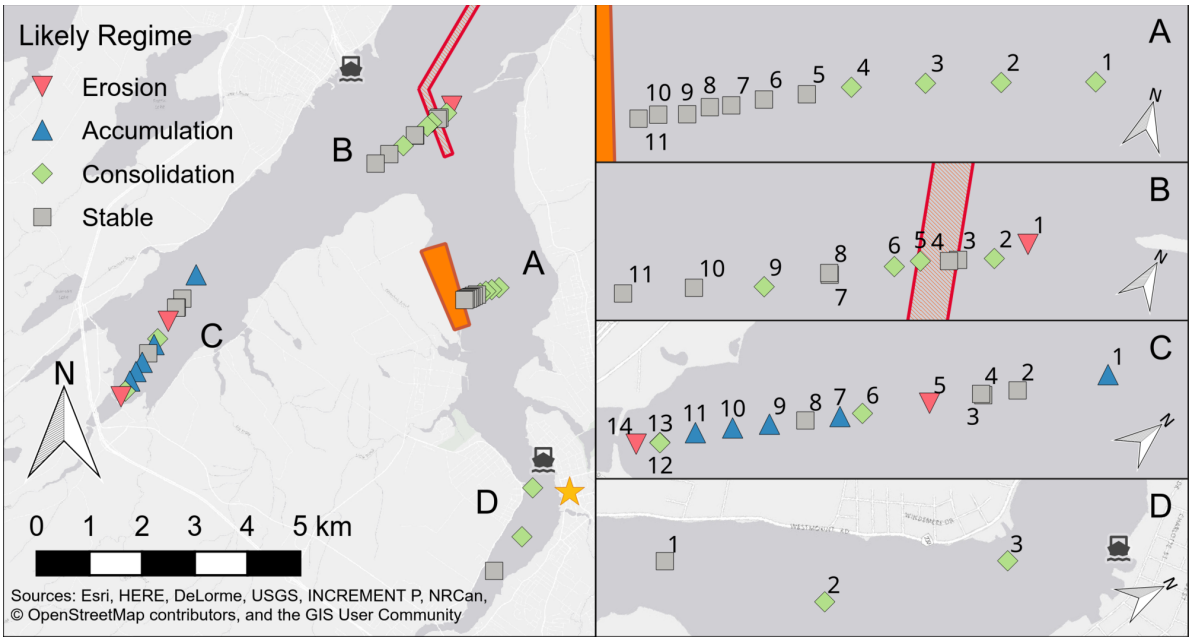

Figure 3.5: Classified trends of sediment accumulation, erosion, consolidation, and stability at repeated deployment locations.

There was a slight increase in TS and corresponding decrease in DP1 at the three locations along *Transect D*, extending from the mouth of the Sydney River to the middle of the South Arm (Fig. 3.4d). Erosion was a possible explanation, but unlikely given the

mild hydrodynamic conditions seen before the second survey relative to those before the first. Instead stability and consolidation was suspected as the cause of the results at these locations (Fig. 3.5).

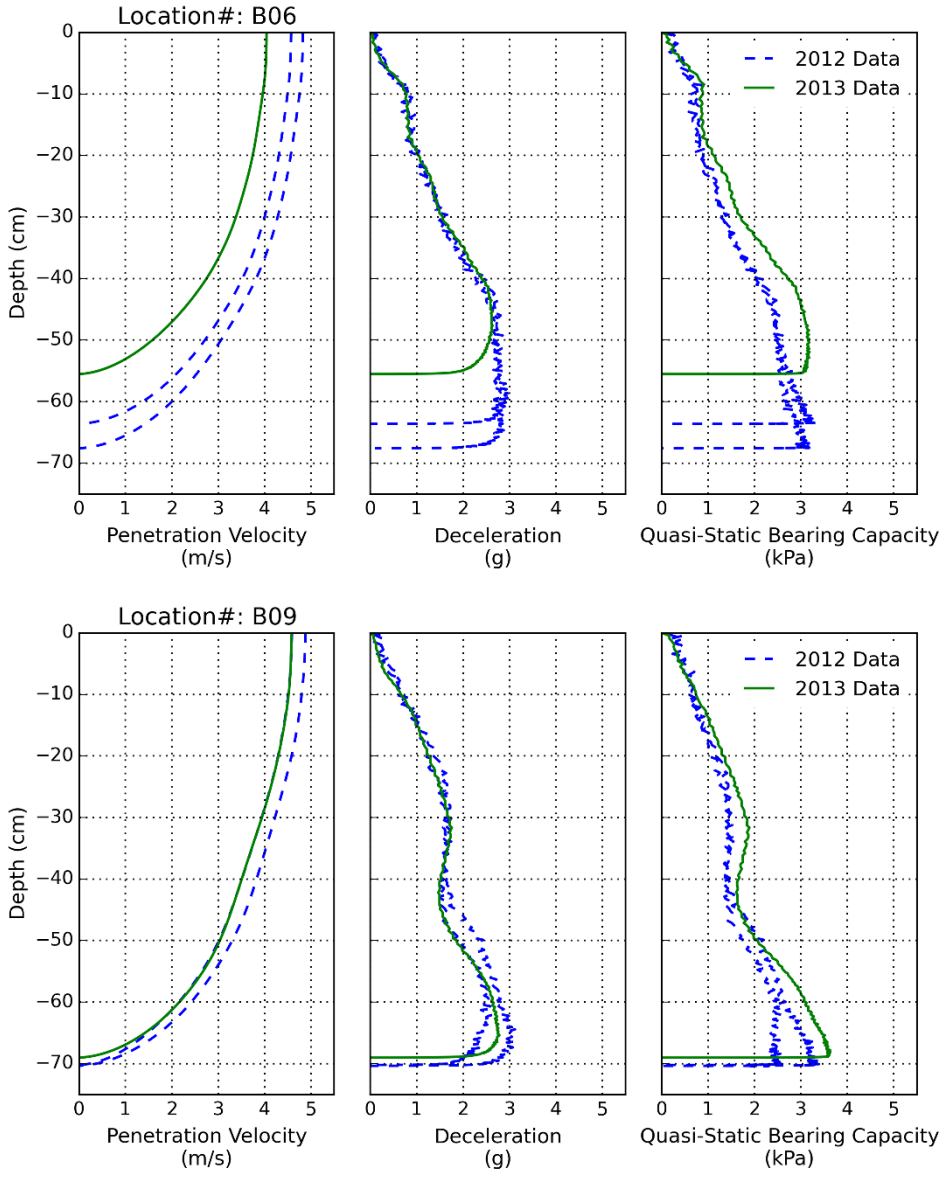

Figure 3.6: Deployment consistency in *Nimrod* results. Deployment locations B06 and B09 in Sydney Harbour demonstrate the level of consistency in survey location, deployment technique, and data processing during the two surveys. The two blue dashed lines represent the two deployments at each location in 2012 while the single green line represents the single deployment made at each location in 2013.

Overall, the high consistency between the *Nimrod* impact velocities in 2012 and 2013 (2012: 4.95 ±0.54 m/s, 2013: 4.57 ±0.68 m/s) gave confidence in the consistent quality of instrument deployments and the results of the study. Two examples of *Nimrod* deployments showing instrument consistency are shown in Fig. 3.6. The high resolution of impacts and consistent deployments in this study allows for the detection of small changes in sediment consolidation state, as is seen in Figure 3.6a.

3.6 Discussion

The combined results of *Nimrod* deployments and sediment consolidation tests indicated erosion at three locations in Sydney Harbour: near the tip of the South Bar (B01), in the middle of the Northwest Arm (C05), and at the outflow of Balls Creek into the Northwest Arm (C14). The latter may be explained if the outflow of Balls Creek still resembles a jet at this location, with the flow still swift enough to avoid sediment deposition. Sediment deposition would become more dominant as flow continues to slow down while entering further into the Harbour. This explanation correlates well with the observed accumulation of sediment at locations C09 to C11 (Fig 3.5). At location B01, flow turbulence with eddy shedding or streamline contraction is likely present due to tidal flow at the tip of South Bar, and may favor erosion at this location. Reasons for the observed trend of erosion at location C05 in the Northwest Arm were unclear, even though the evidence for erosion was the most pronounced in the penetrometer data at this location.

In addition to the three areas of erosion, three areas of ongoing sediment deposition were located in the Northwest Arm of the Harbour at locations C01, C07, and from C09 to C11. Sediment transported from Balls Creek and Leitches Creek could be responsible for the deposition at locations C07 and C09 to C11. These areas are situated just beyond the point where each of the tributaries widens upon merging with the Harbour, leading to a decrease in flow velocity, which would allow suspended sediments to settle out here. The apparent accumulation at C01 could be due to the continuing southward migration of dredge spoil that was initially pushed into the Northwest Arm following dredging (Stark et al. 2014a), due to bed-load transport at this location (Petrie et al. 2001).

The remaining thirty-one survey locations were found to be unchanged, apparently undergoing a natural process of consolidation (Tab. 3). Generally, consolidation of sediment is expected to produce trends in DP1 and TS similar to those seen in areas of erosion. However, erosion was distinguished by observed TS values greater than those expected for normally consolidated sediments. Furthermore, in parts of the Harbour with greater depths and less energetic hydrodynamic conditions, the likelihood of erosion is low.

Table 3.3: Likely initial and final sediment consolidation states derived from *Nimrod* data. Observed changes in the relative consolidation state suggest the likely regime of sediment dynamics taking place for each location in Sydney Harbour.

Location	Initial CS	Final CS	Change TS (kPa)	Change DP1 (cm)	Likely Regime
A01	UC	UC	0.05	-19	Consolidating
A02	UC	UC	0.1	-14	Consolidating
A03	UC	UC	0.05	-9	Consolidating
A04	NC	NC	0.35	-12	Consolidating
A05	NC	NC	0.1	0	Stable
A06	OC	NC	-1	0	Stable
A07	OC	OC	-4	0	Stable
A08	OC	OC	-2	0	Stable
A09	OC	OC	-32	0	Stable
A10	OC	OC	0	0	Stable
A11	OC	OC	0	0	Stable
B01	OC	OC	1	-1	Eroding
B02	NC	NC	0.3	-3	Consolidating
B03	UC	UC	-0.05	0	Stable
B04	UC	UC	0	3	Stable
B05	UC	UC	0.1	-2	Consolidating
B06	UC	UC	0.1	-4	Consolidating
B07	UC	UC	-0.1	-4	Stable
B08	UC	UC	0	-3	Stable
B09	UC	UC	0.1	-3	Consolidating
B10	UC	UC	0	0	Stable
B11	UC	UC	0	0	Stable
C01	UC	UC	-0.1	2	Accumulating
C02	OC	NC	-3	8	Stable
C03	OC	OC	-1	0	Stable
C04	OC	NC	-4	1	Stable
C05	NC	OC	1.5	-1	Eroding
C06	UC	NC	0.1	-1	Consolidating
C07	NC	UC	-0.6	7	Accumulating
C08	NC	NC	0	0	Stable
C09	NC	NC	-0.1	2	Accumulating
C10	NC	UC	-0.7	8	Accumulating
C11	NC	NC	-0.5	2	Accumulating
C12	NC	NC	1	-4	Consolidating
C13	NC	NC	0.7	-2	Consolidating
C14	OC	OC	5	-1	Eroding
D01	UC	UC	0	-2	Stable
D02	UC	UC	0.1	-5	Consolidating
D03	UC	UC	0.1	-6	Consolidating

Note: NC = Normally Consolidated, OC = Over-Consolidated, and UC = Under Consolidated.

The material displaced during dredging in the inner section of the dredged channel is considered to have higher levels of contamination than the sediment introduced by the Harbour's tributaries (Smith et al. 2009). Out of three areas characterized by sediment erosion, just one overlapped with an area of known deposition of dredged material, location C14 near Balls Creek. The observed "softening" of sediments at locations C02-C04 may be attributable to a slow migration and mixing of fine dredged material from the north with the original sediments in this area. The fact that deposits of dredged sediment appeared mostly stable, or were covered and mixed with freshly deposited (post-dredge) sediments, indicates low risks of remobilization or re-exposure of contaminated sediments. Thus, the long-term net effect of dredging on the water quality in the Harbour is likely to be positive (because of increased ventilation), rather than negative because of exposure of contaminated sediments. The apparent stability, combined with the low natural sedimentation rates in Sydney Harbour (Stewart et al. 2001; Lee 2002; Walker et al. 2013a) and the lack of evidence for infilling of the dredge channel at the time of the *Nimrod* surveys, also suggests that no maintenance dredging of the inner part of the dredge channel will be required in the near future. This conclusion is consistent with suggestions made by Jacques Whitford Limited (2009a) and CBCL Limited (2009b) prior to dredging.

The method of identifying areas of erosion and deposition proposed in this study is quite similar to that of Håkanson (1986). That author mapped areas of erosion, transport, and accumulation on the ultimate penetration depth of three different cones deployed from a single instrument. The cones had different bearing areas and were subjected to different loads. In effect, the instrument measured the depth until sediment with a given bearing capacity was reached. While Håkanson's (1986) instrument differs from the *Nimrod* penetrometer used here, the method of evaluating sediment strength at a given depth, or conversely the depth to a given sediment strength, in order to identify areas of erosion and deposition is similar. However, our method of predicting ranges of sediment bearing capacity to estimate sediment consolidation state differs significantly from that used by Håkanson (1986).

One inherent problem with the method of the data analysis used in this study is that it assumes sediment composition is homogeneous with depth. While this assumption may be reasonable in many areas of Sydney Harbour, it is probably a poor assumption in areas where a transition from fine grained to sandy material takes place and layering of different sediments is likely. However, these cases can often be distinguished by sudden changes in the deceleration vs. depth and *qsbc* vs. depth profiles from a deployment (Stoll et al. 2007; Stark and Wever 2009). This allows sediment heterogeneity to be identified and distinct sediment layers to be analyzed separately. This was observed, for example, at location A06 to A11 near the CDF where a thin layer of loose material was present over a much harder substrata.

3.7 Conclusions

Two marine surveys assessed geotechnical characteristics of the uppermost seabed surface to determine sediment remobilization and deposition nine and eighteen months after dredging of a navigation channel and construction of a Confined Disposal Facility in Sydney Harbour. The portable free-fall penetrometer *Nimrod* was used to quantify the strength and thickness of superficial sediment layers in order to identify areas of sediment erosion and accumulation during the period between surveys. Additionally, sediment push cores and grab samples were analyzed for grain-size and classified according to the USCS (united soil classification system). Oedometer tests of sediments from four locations in the Harbour were used to define a range of sediment strength that is likely to be encountered in normally consolidated, homogeneous sediments. The parameters TS (defined as the quasi-static bearing capacity at 10 cm penetration) and DP1 (defined as the depth of penetration until a bearing capacity of 1 kPa is reached) were compared with expected values and used to classify the sediment consolidation state at each impact location. By examining changes in the consolidation state of sediments in the Harbour over time, spatially distributed trends of erosion/deposition and consolidation/reworking were inferred.

The following conclusions can be drawn from the results of this work regarding the sediment dynamics in Sydney Harbour.

1. Three areas of erosion were identified in Sydney Harbour, constituting less than 8% of the thirty-nine *Nimrod* deployment locations examined. Just one of these areas coincided with a previously identified zone of dredged material deposition (C14).

2. Three areas of sediment accumulation were identified representing $\sim 13\%$, or five, of the thirty-nine deployment locations. These were all located in the Northwest Arm (C01, C07, and from C09 to C11).

3. 79% of locations were either consolidating or unchanged.

4. Observed stability at all sites along the inner portion of the dredged navigation channel, including the stormier late fall-winter season, suggests that ongoing maintenance dredging in this part of the Harbour will not be necessary.

5. The bund-wall of the CDF appeared stable between the two surveys, despite evidence of past erosion seen during the first survey.

6. Due to the general stability of dredged material deposits, the long term environmental impact of recent dredging is likely to be positive or negligible.

This research has further explored the types of analyses that can be performed using portable free-fall penetrometer results. Values of K were estimated using empirical relationships and

index properties in this study. However, K could also be found by calibration with field or laboratory data. If penetrometer deployments are made in sediments that are known to be normally consolidated and reliable equilibrium pore pressure measurements are taken after the penetrometer impact is complete, then $\sigma_{vo}{}'$ can be calculated at depth and used to estimate K. In this case, *a priori* knowledge of USR or N_c would be completely unnecessary. With sufficient calibration this could even lead to estimates of *in-situ* void ratios over large areas simply from penetrometer data and index properties.

The sites surveyed during this study only cover the south section of the dredged channel (i.e. transect B) and suggest that ongoing maintenance dredging will not be needed at this location. However, the modeling studies performed by CBCL Limited (2009b) estimated that maintenance dredging would not be required with great frequency even in the seaward end of the dredged channel. Also, the location of an area of sediment mobilization in the Northwest Arm of Sydney Harbour appears to have shifted during the study period. It would be of interest to see how both the seaward end of the dredged channel and the area of sediment mobilization in the Northwest Arm of the Harbour respond to storms and, or high intensity rainfall by surveying before and after major events.

Chapter 4. Conclusions

The results of this work have led to four principal conclusions. First, a method for refining impact detection of FFPs using existing instrumentation has demonstrated that useful information can be obtained for the first few centimeters of impact, prior to full-cone insertion. This directly contrasts with the previous assertions of some authors (e.g. Chow and Airey 2013; Moavenian et al. 2016). The prevalence of this point of view illustrates the need for improved impact detection methods. It is also possible that the observation of deceleration "close to the seabed, but before impact" by Mulhearn (2002) can be explained by issues during impact detection.

Second, a method for inferring consolidation state based on impact profiles and oedometer tests was developed. This demonstrated that it is possible to estimate sediment consolidation state (and potentially *in-situ* density) using the existing *Nimrod* FFP instrumentation without requiring modifications. However, in order to quantify and improve the accuracy of the method developed, further testing needs to be pursued.

Third, a method for identifying areas of potential sediment erosion and deposition was proposed. This third method was developed as an extension of the previous two methods while also considering the results of oedometer tests conducted on sediment samples taken from the field. The accuracy and reliability of this method still needs to be quantified through further testing and calibration.

Finally, by using the methods developed in this work approximately 79% of the locations surveyed in Sydney Harbour were found to have been stable or consolidating over the course of the eighteen months following dredging in the winter of 2012-13. Areas of erosion and deposition were identified by first accurately identifying the point where the FFP begins to enter the seabed and then inferring sediment consolidation state by comparing observed *qsbc* values to ideal values for fully self-weight consolidated sediment. Areas with over-consolidated surface sediments were considered to be eroding, while areas of not quite fully-consolidated sediment were considered stable or accumulating. Stability and accumulation were distinguished depending on how consolidation progressed over the study period. The

observed stability of surficial seabed sediments in the South and Northwest Arms of Sydney Harbour agrees the hydrodynamic and sediment dynamic conditions in the harbor (e.g. Petrie et al. 2001; Stewart et al. 2001; Lee 2002; Walker et al. 2013a).

The results in this work were obtained using newly developed methods for identifying FFP impact with the seabed and for inferring *in-situ* sediment consolidation state from observed *qsbc*-depth profiles at each impact location. The inferred sediment consolidation state was based on the assumption of undrained conditions in uniform fine-grained material. While these assumptions were considered to be valid for the sediments and penetrometer impact velocities encountered in this study, they are not universally applicable.

This thesis represents an initial effort to develop methods to improve seafloor impact detection, infer sediment consolidation, and map area of erosion and deposition using portable free-fall penetrometers. Due to the novelty of these techniques, the next steps in continuing this work must include calibration in a controlled laboratory environment. Ideally, this work would occur under conditions mimicking those in the field as closely as possible. Such conditions may be obtained through the use of a CPT calibration chamber.

In a calibration chamber it is possible to control the boundary stress conditions or boundary strain conditions in a soil element. Also things like temperature, salinity, soil composition, and hydraulic gradients may be controlled and quantified as well. Additionally, deceleration measurements made by the FFP can be verified via secondary methods such as photogrametry (e.g. Chow and Airey 2013). The calibration chamber at Virginia Tech is capable of forming cylindrical soil samples six feet in diameter by six feet tall. It is also designed to simulate pressures up to the equivalent of a 300 meter water column, making it an ideal facility for laboratory calibration of these new methods. Figure 4.1 below shows a scale drawing of the *Nimrod* FFP in the calibration chamber ready for deployment.

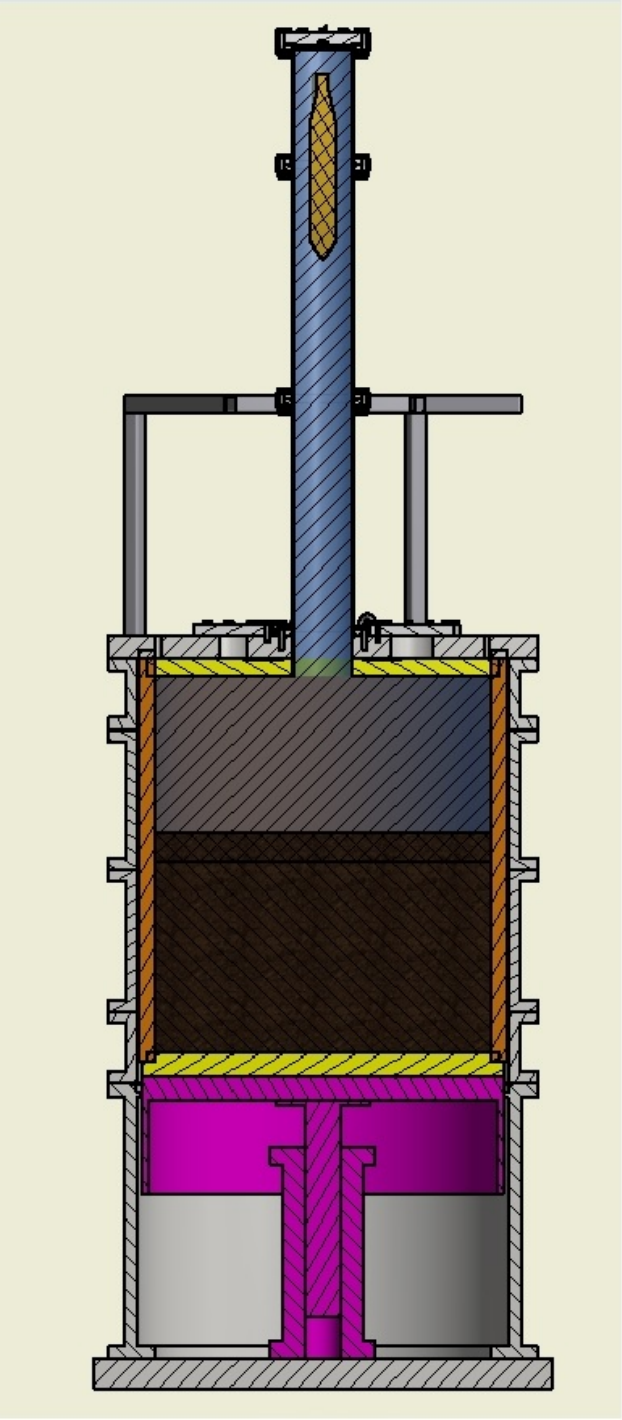

Figure 4.1: The new USACE/VT CPT calibration chamber. The *Nimrod* FFP is shown prepared for deployment.

References

Anderson, J.D. (1995). Computational fluid dynamics: the basics with applications. New York: McGraw-Hill.

Ashley, G.M. (1990). Classification of large-scale subaqueous bedforms: a new look at an old problem-SEPM bedforms and bedding structures. *J. Sediment. Petrol.*, 60(1), 160-172.

ASTM D2435 / D2435M-11 (2011). Standard Test Methods for One-Dimensional Consolidation Properties of Soils Using Incremental Loading. ASTM International, West Conshohocken, PA. (www.astm.org).

ASTM D2487-11 (2011). Standard Practice for Classification of Soils for Engineering Purposes (Unified Soil Classification System), ASTM International, West Conshohocken, PA. (www.astm.org).

ASTM D5/D5M-13 (2013). Standard Test Method for Penetration of Bituminous Materials, ASTM International, West Conshohocken, PA. (www.astm.org).

ASTM D5778-12 (2012). Standard Test Method for Electronic Friction Cone and Piezocone Penetration Testing of Soils. ASTM International, West Conshohocken, PA. (www.astm.org).

Aubeny, C.P., Shi, H. (2006). Interpretation of impact penetration measurements in soft clays. *J. Geotech. Geoenviron.*, 132(6), 770-777.

Blake, A. P., O'Loughlin, C. D., Morton, J. M., O'Beirne, C., Gaudin, C., White, D. J. (2016). In-situ measurement of the dynamic penetration of free-fall projectiles in soft soils using a low cost inertial measurement unit. *Geotech. Test. J.*.[In press].

Boggess, R., Robertson, P.K. (2011). CPT for soft sediments and deepwater investigations. In: *Offshore Technology Conference*. Offshore Technology Conference.

Booij, N., Holthuijsen, L.H., and Ris, R.C. (1996). The "SWAN" wave model for shallow water. *Coastal Engineering Proceedings*, 1(25).

Caple, M., James, I., Bartlett, M. (2012). Mechanical behaviour of natural turf sports pitches across a season. *Sports Engineering*, 15(3), 129-141.

Carrier, W.D., III, Bromwell, L.G., and Somogyi, F. (1983). Design capacity of slurried mineral waste ponds. *J. Geotech. Engrg.*, 109(5), 699-716.

Carter, J.P., Nazem, M. (2013). Analysis of dynamic penetration of soils. *American Environmentalism: Philosophy, History, and Public Policy*, 3-13.

CBCL Limited (2009a). Physical Oceanography. In: Environmental Assessment for Sydney Harbour Access Channel Deepening and Sydport Container Terminal. Final Report, Appendix D. Jacques Whitford Limited. Laurentian Energy Corp. (http://www.gov.ns.ca/nse/ea/sydney.harbour.terminal/Appendix_D.pdf). Accessed 14 December 2015.

CBCL Limited (2009b). Plume and deposition modeling. In: Environmental Assessment for Sydney Harbour Access Channel Deepening and Sydport Container Terminal. Final Report, Appendix A. Jacques Whitford Limited. Laurentian Energy Corp. (http://www.gov.ns.ca/nse/ea/sydney.harbour.terminal/Appendix_A.pdf) Accessed 14 December 2015.

Cherrett, J.M. (1968). A simple penetrometer for measuring leaf toughness in insect feeding studies. *J. Econ. Entomol.*, 61(6), 1736-1738.

Chow, S.H., Airey, D.W. (2013). Soil strength characterization using free-falling penetrometers. *Géotechnique*, 63(13), 1131-1143.

Chow, S.H., O'Loughlin, C.D., Randolph, M.F. (2014). Soil strength estimation and pore pressure dissipation for free-fall piezocone in soft clay. *Géotechnique*, 64(10), 817-827.

Chung, S. F., Randolph, M. F., Schneider, J. A. (2006). Effect of penetration rate on penetrometer resistance in clay. *J. Geotech. Geoenviron.*, 132(9), 1188-1196.

Dasari, G.R., Karthikeyan, M., Tan, T.S., Mimura, M., Phoon, K.K. (2006). In Situ Evaluation of Radioisotope Cone Penetrometers in Clays. *Geotech. Test. J.*, 29(1) 45-53.

Dayal, U., Allen, J. H. (1973). Instrumented impact cone penetrometer. *Can. Geotech. J.*, 10(3), 397-409.

Dayal, U., Allen, J. H., Jones, J. M. (1975). Use of an impact penetrometer for the evaluation of the insitu strength of marine sediments. *Mar. Georesour. Geotec.*, 1(2), 73-89.

Dayal, U. (1981). Analysis of free-fall penetrometer data. In: *OCEANS 81* (683-687) IEEE.

Denness, B., Berry, A., Darwell, J., Nakamura, T. (1981). Dynamic seabed penetration. In: *OCEANS 81* (662-667) IEEE.

Dijkstra, J., Broere, W., van Tol, A.F. (2012). Electrical resistivity method for the measurement of density changes near a probe. *Géotechnique*, 62(8), 721-725.

Dorvinen, J., Stark, N., Hatcher, B., Hatcher, M., Leys, V., Kopf, A. (2015). *In-situ* geotechnical investigation of a confined sediment disposal facility, Sydney Harbour, Nova Scotia. In: *Proceedings of Coastal Sediments 2015, San Diego, CA*.

García, M. (2008). Sediment Transport and Morphodynamics. *Sedimentation Engineering*, 21-163.

Glaser, D.L., Ball, A.J., Zacny, K.A. (2008). A review of penetrometers for subsurface access on comets and asteroids. *Meteorit. Planet. Sci.*, 43(6), 1021-1032.

Gregory, D., Petrie, B., Jordan, F., Langille, P. (1993). Oceanographic, geographic, and hydrological parameters of Scotia-Fundy and southern Gulf of St. Lawrence inlets. Bedford Institute of Oceanography. Dartmouth, Nova Scotia. (http://www.dfo-mpo.gc.ca/Library/143396.pdf) Accessed 14 December 2015.

Ha, H.K., Maa, J.P.Y., Holland, C.W. (2010). Acoustic density measurements of consolidating cohesive sediment beds by means of a non-intrusive "Micro-Chirp" acoustic system. *Geo-Marine Letters*, 30(6), 585-593.

Ha, H.K., Maa, J.P.Y., Park, K., Kim, Y.H., (2011). Estimation of high-resolution sediment concentration profiles in bottom boundary layer using pulse-coherent acoustic Doppler current profilers. *Marine Geology*, 279(1-4), 199-209.

Haghighat, A. (2014). Monte Carlo Methods for Particle Transport. CRC Press.

Harker, F.R., Maindonald, J.H., Jackson, P.J. (1996). Penetrometer measurement of apple and kiwifruit firmness: operator and instrument differences. *J. Am. Soc. Hortic. Sci.*, 121(5), 927-936.

Harris, M.M., Avera, W.E., Abelev, A., Bentrem, F.W., Bibee, L.D. (2008). Sensing shallow seafloor and sediment properties, recent history. In: *IEEE Oceans 2008, Quebec City, QC*, 1-11.

Hirst, T.J., Perlow, M., Richards, A.F., Burton, B.S., Van Sciver, W.J. (1975). Improved in situ gamma-ray transmission densitometer for marine sediments. *Ocean Engineering*, 3(1), 17-27.

Hvorslev, M.J. (1961). Physical Components of the Shear Strength of Saturated Clays (No. WES-MP-3-428). Army Engineer Waterways Experiment Station Vicksburg, MS.

Håkanson, L. (1986). A sediment penetrometer for in situ determination of sediment type and potential bottom dynamic conditions. *Internationale Revue der gesamten Hydrobiologie und Hydrographie*, 71(6), 851-858.

Irish, J.L., White, T.E. (1998). Coastal engineering applications of high-resolution lidar bathymetry. *Coastal Engineering*, 35(1), 47-71.

Jacques Whitford Limited (2009a). Overview of the Environment. In: Environmental Assessment for Sydney Harbour Access Channel Deepening and Sydport Container Terminal. Final Report, Section 4. Jacques Whitford Limited. Laurentian Energy Corp. (http://www.gov.ns.ca/nse/ea/sydney.harbour.terminal/Section04.pdf) Accessed 14 December 2015.

Jacques Whitford Limited (2009b). Environmental Assessment for Sydney Harbour Access Channel Deepening and Sydport Container Terminal. Jacques Whitford Limited. Laurentian Energy Corp. Project No. 1041307. Final Report. (http://www.novascotia.ca/nse/ea/sydney.harbour.terminal.asp) Accessed 14 December 2015.

Jia, R., Hino, T., Hamada, T., Chai, J., Yoshimura, M. (2013a). Density and undrained shear strength of bed sediment from ND-CPT. *Ocean Dynamics*, 63(1), 507-517.

Jia, R., Hino, T., Chai, J., Hamada, T., Yoshimura, M. (2013b). Interpretation of density profile of seabed sediment from nuclear density cone penetration test results. *Soils and Foundations*, 53(5), 671-679.

Ju, J.W., Cheong, G.H., Kim, Y.G. (2003). Consolidation Characteristics of Dredged Soil with High Water Content. *Magazine of the Korean Society of Agricultural Engineers*, 45(5), 133-139.

Karthikeyan, M., Tan, T.S., Mimura, M., Yoshimura, M., Tee, C.P. (2007). Improvements in Nuclear-Density Cone Penetrometer for Non-Homogeneous Soils. *Soils and Foundations*, 47(1) 109-117.

Keller, G.H. (1965). Deep-sea nuclear sediment density probe. *Deep-Sea Research*, 12(1) 373-376.

Kopf, A., Stegmann, S., Krastel, S., Förster, A., Strasser, M., Irving, M. (2007). Marine deep-water free-fall CPT measurements for landslide characterization off Crete, Greece (Eastern Mediterranean Sea) Part 2: Initial data from the Western Cretan Sea. In: *Submarine mass movements and their consequences* 199-208, Springer Netherlands.

Lee, K., Yeats, P., Smith, J., Pertie, B., Milligan, T.G. (2002). Environmental effects and remediation of contaminants in Sydney Harbour, NS. TSRI Project, (93). (http://www.ceaa.gc.ca/050/documents_staticpost/cearref_8989/MISC-130.pdf) Accessed 14 December 2015.

Lund, R.J. (1990). Scheduling maintenance dredging on a single reach with uncertainty. *J. Waterw. Port. C-ASCE*, 116(2), 211-231.

Lunne, T., Robertson, P.K., Powell, J.J.M. (1997). Cone penetration testing. *Geotechnical Practice*.

Lunne, T. (2012). The Fourth James K. Mitchell Lecture: The CPT in offshore soil investigations - a historic perspective. *Geomechanics and Geoengineering*, 7(2), 75-101.

McAnally, W.H., Friedrichs, C., Hamilton, D., Hayter, E., Shrestha, P., Rodriguez, H., Sheremet, A., Teeter, A. (2007a). Management of fluid mud in estuaries, bays, and lakes. I: Present state of understanding on character and behavior. *J. Hydraul. Eng-ASCE.*, 133(1), 9-22.

McAnally, W. H., Teeter, A., Schoellhamer, D., Friedrichs, C., Hamilton, D., Hayter, E.,

Shrestha, P., Rodriguez, H., Sheremet, A., Kirby, R. (2007b). Management of fluid mud in estuaries, bays, and lakes. II: Measurement, modeling, and management. *J. Hydraul. Eng-ASCE.*, 133(1), 23-38.

McCalla, R.J. (1999). Global change, local pain: intermodal seaport terminals and their service areas. *J. Transp. Geogr.* 7(4), 247-254.

Mesri, G. (1989). A reevaluation of su(mob) = 0.22σ'p using laboratory shear tests. *Can. Geotech. J.*, 26(1), 162-164.

Moavenian, M.H., Nazem, M., Carter, J.P., Randolph, M.F. (2016). Numerical analysis of penetrometers free-falling into soil with shear strength increasing linearly with depth. *Computers and Geotechnics*, 72(1), 57-66.

Monte, J.L., Krizek, R.J. (1976). One dimensional mathematical model for large strain consolidation. *Géotechnique*, 26(3), 495-510.

Morton, J.P., O'Loughlin, C., White, D. (2015). Centrifuge modelling of an instrumented free-fall sphere for measurement of undrained strength in fine-grained soils. *Can. Geotech. J.*. (http://dx.doi.org/10.1139/cgj-2015-0242) Accessed 7 March 2016.

Morris, P.H. (2007). Correlations for Zero Effective Stress Void Ratio of Fine-Grained Marine and Riverine Sediments. *J. Waterw. Port. C-ASCE*, 133(4) 305-308.

Mosher, D.C., Christian, H., Cunningham, D., MacKillop, K., Furlong, A., Jarrett, K. (2007). The Harpoon free fall cone penetrometer for rapid offshore geotechnical assessment. In: *Offshore Site Investigation and Geotechnics, Confronting New Challenges and Sharing Knowledge*. Society of Underwater Technology.

Mulhearn, P.J. (2002). Influences of penetrometer probe tip geometry on bearing strength estimates for mine burial prediction (No. DSTO-TR-1285). Defence Science and Technology Organization Canberra, Australia. (http://www.dtic.mil/dtic/tr/fulltext/u2/a402610.pdf) Accessed March 5, 2016.

Mulhearn, P. J. (2003). Influences of penetrometer tip geometry on bearing strength estimates. *Int. J. Offshore Polar*, 13(01).

Mulukutla, G.K., Huff, L.C., Melton, J.S., Baldwin, K.C., Mayer, L.A. (2011). Sediment identification using free fall penetrometer acceleration-time histories. *Mar. Geophys. Res.*, 32(3), 397-411.

Petrie, B., Bugden, G., Tedford, T., Geshelin, Y., Hannah, C. (2001). Review of the physical oceanography of Sydney Harbour. Bedford Institute of Oceanography. Dartmouth, Nova Scotia. (http://www.dfo-mpo.gc.ca/Library/315795.pdf) Accessed 14 December 2015.

Oliveira, J. R., Almeida, M. S., Motta, H. P., Almeida, M. C. (2011). Influence of penetration rate on penetrometer resistance. *J. Geotech. Geoenviron.*, 137(7), 695-703.

Osler, J., Furlong, A., Christian, H. (2006). A sediment probe for the rapid assessment of seabed characteristics. In: *Acoustic sensing techniques for the shallow water environment*, 171-181.

Parker, W., Kirby, R. (1981). Time dependent properties of cohesive sediment relevant to sedimentation management: European experience. Estuarine Comparisons 1982. In: *Proceedings of the Sixth Biennial International Estuarine Research Conference*, 573-589.

Poeckert, R.H., Preston, J.M., Miller, T., Relega, R., Eastgaard, A. (1997). A seabed penetrometer. DREA Technical Memorandum 97/233.

Rapaglia, J., Zaggia, L., Ricklefs, K., Gelinas, M., Bokuniewicz, H. (2011). Characteristics of ships' depression waves and associated sediment resuspension in Venice Lagoon, Italy. *J. Marine Syst.*, 85(1), 45-56.

Robertson, P.K., Campanella, R.G. (1983). Interpretation of cone penetration tests. Part II: Clay. *Can. Geotech. J.*, 20(4), 734-745.

Robertson, P.K. (2009). Interpretation of cone penetration tests-a unified approach. *Can. Geotech. J.*, 46(11), 1337-1355.

Seifert, A., Kopf, A. (2012). Modified dynamic CPTU penetrometer for fluid mud detection. *J. Geotech. Geoenviron.*, 138(2), 203-206.

Shibata, T., Mimura, M., Shrivastava, A.K., Nobuyama, M. (1992). Moisture Measurement by Neutron Moisture Cone Penetrometer: Design and Application. *Soils and Foundations*, 32(4) 58-67.

Skempton, A.W. (1951). The bearing capacity of clays. *Building Research Congress* 1(1), 180-189.

Skempton, A.W. (1970). The consolidation of clays by gravitational compaction. *Quarterly Journal of the Geological Society of London*, 125(1), 373-411.

Smith, J.N., Lee, K., Gobeil, C., Macdonald, R.W. (2009). Natural rates of sediment containment of PAH, PCB and metal inventories in Sydney Harbour, Nova Scotia. *Sci. Total Environ.*, 407(17), 4858-4869.

Stark, N., Kopf, A., Hanff, H., Stegmann, S., Wilkens, R. (2009a). Geotechnical investigations of sandy seafloors using dynamic penetrometers. In: *Oceans 2009, MTS/IEEE Biloxi-Marine Technology for Our Future - Global and Local Challenges*, 1-10.

Stark, N., Hanff, H., Kopf, A. (2009b). Nimrod: a tool for rapid geotechnical characterization of surface sediments. *Sea Technology*, 50(4), 10-14.

Stark, N., Wever, T.F. (2009). Unraveling subtle details of expendable bottom penetrometers (XBP) deceleration profiles. *Geo-Marine Letters*, 29(1), 39-45.

Stark, N., Kopf, A. (2011). Detection and quantification of sediment remobilization processes

using a dynamic penetrometer. In: *Proceedings of IEEE Oceans 2011*, 1-9.

Stark, N., Wilkens, R., Ernstsen, V.B., Lambers-Huesmann, M., Stegmann, S., Kopf, A. (2012). Geotechnical properties of sandy seafloors and the consequences for dynamic penetrometer interpretations: quartz sand versus carbonate sand. *Geotechnical and Geological Engineering*, 30(1), 1-14.

Stark, N., Hatcher, B., Hatcher, M., Leys, V., Kopf, A. (2014a). *In-situ* localization and quantification of sediment deposits after dredging and disposal interventions in Sydney Harbour, Canada, using a dynamic penetrometer. In: *Geo-Congress 2014*, 2122-2133.

Stark, N., Staelens, P., Hay, A.E., Hatcher, B., Kopf, A. (2014b). Geotechnical investigation of coastal areas with difficult access using portable free-fall penetrometers. In: 3^{rd} *International Symposium on Cone Penetration Testing, Las Vegas, Nevada, USA*, 231-238.

Stark, N., Quinn, B., Ziotopoulou, K., Lantuit, H. (2015). Geotechnical Investigation of Pore Pressure Behavior of Muddy Seafloor Sediments in an Arctic Permafrost Environment. In: *ASME 2015 34th International Conference on Ocean, Offshore and Arctic Engineering* American Society of Mechanical Engineers.

Stegmann, S., Mörz, T., Kopf, A. (2006). Initial Results of a new Free Fall-Cone Penetrometer (FF-CPT) for geotechnical in-situ characterisation of soft marine sediments. *Norsk Geologisk Tidsskrift*, 86(3), 199-208.

Steiner, A., Kopf, A. J., L'Heureux, J. S., Kreiter, S., Stegmann, S., Haflidason, H., Moerz, T. (2013). In situ dynamic piezocone penetrometer tests in natural clayey soils - a reappraisal of strain-rate corrections. *Can. Geotech. J.*, 51(3), 272-288.

Stephan, S., Kaul, N., Stark, N., Villinger, H., Wever, T. (2011). LIRmeter: a new tool for rapid assessment of sea floor parameters. Bridging the gap between free-fall instruments and frame-based CPT. In: *OCEANS 2011*, 1-10.

Stewart, A.R.J., Milligan, T., Law, B., Loring, D. (2001). Disaggregated inorganic grain size and trace metal analysis of surficial sediments in Sydney Harbour, N. S., 1999. *Can. Tech. Rep. Fish. Aquat. Sci.* (http://publications.gc.ca/collections/collection_2014/mpo-dfo/Fs97-6-2384-eng.pdf) Accessed 14 December 2015.

Stoll, R. D., Akal, T. (1999). XBP- Tool for Rapid Assessment of Seabed Sediment Properties. *Sea Technology*, 40(2), 47-52.

Stoll, R.D. (2004). Measuring sea bed properties using static and dynamic penetrometers. In: *Civil Engineering in the Oceans VI*, 386-395.

Stoll, R.D., Sun, Y.F., Bitte, L. (2007). Seafloor properties from penetrometer tests. *IEEE Journal of Oceanic Engineering*, 32(1), 57-63.

Terzaghi, K. (1943). Theoretical soil mechanics. Wiley.

Thomson, R.E., Emery, W.J. (2014). Data analysis methods in physical oceanography. Amsterdam: Elsevier Science.

Thompson, D., March, R., Herrmann, H. (2002). Groundtruth results for dynamic penetrometers in cohesive soils. In: *OCEANS'02 MTS/IEEE* (Vol. 4) 2117-2123.

United States National Ocean Service, & United States National Oceanic and Atmospheric Administration (2016). NOS hydrographic surveys specifications and deliverables. Silver Spring, MD: U.S. Dept. of Commerce, National Oceanic and Atmospheric Administration.

United States Army Corps of Engineers (1983). Dredging and Dredged Material Disposal. EM 1110-2-5025. Chapter 4. (http://www.publications.usace.army.mil/Portals/76/Publications/EngineerManuals/EM_1110-2-5025.pdf) Accessed 14 December 2015.

van Craenenbroeck, K., Duthoo, O., Vandecasteele, M., Eygenraam, J., van Oostveen, J. (1998). Application of modern survey techniques in today's dredging practice. *Terra et Aqua*, 72(1), 3-9.

Walker, T.R., MacAskill, D., Rushton, T., Thalheimer, A., Weaver, P. (2013a). Monitoring effects of remediation on natural sediment recovery in Sydney Harbour, Nova Scotia. *Environ. Monit. Assess.*, 185(10), 8089-8107.

Walker, T.R., MacAskill, D., Weaver, P. (2013b). Environmental recovery in Sydney Harbour, Nova Scotia: Evidence of natural and anthropogenic sediment capping. *Mar. Pollut. Bull.*, 74(1), 446-452.

Wendt, J.F., Anderson, J.D. (2009). Computational fluid dynamics an introduction. Berlin: Springer.

Winterwerp, J.C., Van Kesteren, W.G. (2004). Introduction to the physics of cohesive sediment dynamics in the marine environment (Vol. 56) Elsevier.

Young, A. C., Babb, L. V., Boggess, R. L. (1988). Mini-probes: A new dimension in offshore in situ testing. In: *OCEANS'88 A Partnership of Marine Interests*, 423-427.